

MAPPING BOTTOMFAST SEA ICE IN ARCTIC LAGOONS USING SENTINEL-1 INTERFEROMETRY

By

Jacob W. Pratt

A Thesis Submitted in Partial Fulfillment of the Requirements

for the Degree of

Master of Science

in

Geophysics

University of Alaska Fairbanks

August 2022

APPROVED:

Andy Mahoney, Committee Chair

Katrin Iken, Committee Member

Jeremy Kasper, Committee Member

Vladimir Romanovsky, Committee Member

Paul McCarthy, Chair, Department of

Geosciences

Karsten Hueffer, Interim Dean, College of

Natural Science and Mathematics

Richard Collins, Director of the Graduate School

Abstract

Sea ice is an important component of Arctic coastal ecosystems. Where the water is shallow enough, it can extend all the way to the seafloor and become bottomfast sea ice (BSI), the lateral extent of which depends upon ice thickness and the regional nearshore slope. Sea ice thickness is a well-known indicator of climate change in the Arctic and in areas with gently sloping seafloors, we expect the extent of BSI to be a sensitive indicator of changes in ice thickness. Contact with the seafloor can help cool and aggregate subsea permafrost and restrict under-ice habitats. It also prevents or reduces motion experienced by floating landfast ice in response to wind, ocean, and ice forcing. Bottomfast ice is in turn more stable than floating ice with implications for human activities on ice. BSI cannot easily be distinguished from floating landfast ice using optical imagery and synthetic aperture radar (SAR) is not typically able to penetrate to the bottom of saline ice. As a result, large-scale mapping of BSI has previously been limited to brackish waters near Arctic deltas, where (SAR) can detect the ice-water interface. However, recent work has demonstrated that SAR interferometry (InSAR) can be used to delineate BSI based on an absence of small-scale surface motion over time. Here, we utilize the Alaska Satellite Facility's Hybrid Pluggable Processing Pipeline (HyP3): A cloud-based infrastructure to process interferograms from the entire Sentinel-1 record over three lagoon systems across the Beaufort Sea coast of Alaska near Utqiagvik, Prudhoe Bay, and Kaktovik. We develop and test a mapping approach that discriminates bottomfast ice based on a near-zero gradient in interferometric phase change, which on floating lagoon ice is primarily caused by surface motion from tides and thermal stress. This enables the comparison of the date of onset, maximum extent, and seasonal evolution of BSI between the lagoons from 2016-2020. We also evaluate the use of electromagnetic sounding in tandem with in-situ drilling to verify BSI extent with greater detail. Based on this work, we argue that mapping BSI could significantly improve our understanding of Arctic lagoons in terms of detailed bathymetry, winter

habitats, and saline stress on benthic communities, and the thermal regime of the underlying permafrost.

Table of Contents

	Page
Abstract.....	iii
Page.....	v
List of figures.....	vii
List of tables	ix
1 Introduction	1
2 Methods and Data	6
2.1 Study regions.....	6
2.2 Detecting BSI using SAR interferometry	7
2.3 Detecting BSI using electromagnetic (EM) sounding.....	9
2.4 Drill hole observations	10
2.5 Ice and sediment coring.....	12
2.6 Freezing degree days	13
3 Results	13
3.1 Transect data	13
3.1.1 Overview of transects in Elson Lagoon	13
3.1.2 Drill-hole data	20
3.1.3 EM conductivity data along transects.....	21
3.1.4 InSAR data along transects	22
3.2 Seasonal progression and interannual variability of BSI extent	25
3.2.1 Overview of InSAR-derived BSI extent.....	25
3.2.2 Elson Lagoon	29
3.2.3 Simpson Lagoon and Stefansson Sound	30
3.2.4 Kaktovik, Jago, and Avery lagoons	31
3.3 Bottom fast ice core observations	32
4 Discussion.....	36
4.1 Validation of InSAR-derived BSI extent.....	36
4.1.1 Detection of BSI vs floating ice	36
4.1.2 Distinction between bonded and unbonded BSI	36
4.2 Assessment of EM conductivity profiling for detecting BSI	40
4.3 Quality of detection for each observation method	40

4.3.1 Interferometric phase values.....	40
4.3.2 Coherence values.....	40
4.3.3 Conductivity values.....	41
4.4 Spatial and temporal variation.....	41
4.5 Submarine permafrost impacts.....	43
4.6 Ecological impacts.....	43
Conclusion.....	44
References.....	49

Figure 1. Idealized cross-sections of the bottomfast ice zone at different times of year, and under different sea level states. Sea level can be affected by a number of variables such as changes in tides, strong winds, or winter storm events. a) Early winter with BSI found only in shallowest water and with a single, active tide crack. b) Late-winter with maximum BSI extent and both inactive and active tide cracks. c) A low-water scenario where both BBSI and UBSI are in contact with the sea floor and only the floating sea ice has a layer of sea water beneath it. d) A high-water scenario in which while the BBSI remains securely frozen to the seafloor, but the UBSI has been lifted from the seafloor allowing sea water to circulate beneath. This temporary detachment is what separates BBSI from UBSI and the period when UBSI is in contact with the ground separates UBSI from floating sea ice which always has a layer of sea water beneath it. 2

Figure 2 Schematic of major lagoon system components (labeled black) and tools (labeled red) to support Beaufort Lagoon Ecosystems (BLE) LTER research..... 4

Figure 3 Five zones representing a typically nearshore environment in Beaufort Sea coastal lagoon system. Zone 1 is the backshore, which has a thin seasonally thawed active layer above near-surface land permafrost. Zone 2 is the beach just before it begins to reach sea ice. Zone 3 is the bottomfast sea ice zone, which is where we aim to define the distinction between areas of BBSI closest to the shore and frozen to the seafloor and the UBSI zone farther seaward where sea ice is unbonded to the seafloor. Zones 4 and 5 represent regions of floating sea ice where the bottom of the ice layer never contacts the seafloor. The seasonally thawed active layer remains relatively thin in zones 1-3 as ice contact with the seafloor prevents year-round exposure to warmer seawater and a talik formation, unlike for zones 4 and 5, which is why there is a steep increase in talik layer thickness following the BSI zone. 5

Figure 4 Map of major river systems associated with each lagoon. (A) The Deadhorse nodes features five major river. (B) Elson Lagoon has no major river system but a few small drainage basins. (C) Kaktovik region features three major river systems. 7

Figure 5 Auger hole transect locations relative to BSI extent as determined by InSAR in grey and red hash marks identifying the boundary between BSI and floating ice determined by drill hole observations. BSI extent was identified from interferograms collected between Apr 30th 2021 and May 12th 2021. Location of sediment core collection is marked with a red dot. Grey shaded region represents BSI extent at the time of collection. Sediment core #1 was collected April 24th, 2021, and sediment core #2 was collected April 25th, 2021. 15

Figure 6 Detailed analysis of transect A along the middle of the shallow shoal in western Elson lagoon across 20 auger holes collected May 1st, 2021. (a) Thickness of floating and unbonded BSI along with thickness measurements for snow, sea ice, and water at each auger location along the transect. (b) Conductivity values from three frequencies 100 kHz, 4000 kHz, and 16000 kHz. T1 identifies the transition from floating sea ice to UBSI and T2 identifies the transition from UBSI back to floating sea ice. (c) Phase values obtained from interferograms. (d) Coherence values. D1 and D2 identify the lowest drops in coherence. 16

Figure 7 Detailed analysis of transect B along the base of the shallow shoal in western Elson lagoon across 19 auger holes collected May 2nd, 2021. (a) Thickness of floating and unbonded BSI along with thickness measurements for snow, sea ice, and water at each auger location along the transect. (b) Conductivity values from three frequencies 100 kHz, 4000 kHz, and 16000 kHz. T1 identifies the transition from floating sea ice to UBSI and T2 identifies the transition from UBSI back to floating sea ice. (c) Phase values obtained from interferograms. (d) Coherence values. D1 and D2 identifies the lowest drops in coherence. 17

Figure 8 Detailed analysis of transect C along a nearshore embayment in western Elson lagoon across 12 auger holes collected April 29th, 2021. (a) Thickness of floating and unbonded BSI along with thickness measurements for snow, sea ice, and water at each auger location along the transect. (b) Conductivity values from three frequencies 100 kHz, 4000 kHz, and 16000 kHz. T1 identifies the transition from land to BBSI and T2 identifies the transition from UBSI to floating sea ice. (c) Phase values obtained from interferograms. (d) Coherence values. Drop identifies the lowest coherence value. 18

Figure 9 Detailed analysis of transect D across the nearshore and a shallow drainage basin. 10 auger holes collected May 5th, 2021. (a) Shows which areas are floating bonded and unbonded along with thickness measurements for snow, sea ice, and water at each auger location. (b) Conductivity values from three frequencies 100 kHz, 4000 kHz, and 16000 kHz. T1 identifies the transition from land to BBSI and T2 identifies the transition from UBSI to floating sea ice. (c) Phase values obtained from interferograms. (d) Coherence values. Drop identifies the lowest coherence value. 19

Figure 10 (a) BSI extent for April 30th, 2021 identified using InSAR based on phase values and the location of drill hole transects. (b) Visual representation of coherence data collected at the same date and location within Elson Lagoon. Coherence values range from 0 (black) to 1 (white). (c) Visual representations of phase values that panel a was based on. Phase values range from 0 (red) to 2π (blue). (d) Bathymetry data at the same location with red being the shallowest regions and blue being waters greater than 2 m depth. 23

Figure 11 Boundaries set for each study region used to calculate the total area extent for each node respectively. 26

Figure 12 Freezing degree day (FDD) calculations for each node. The x axis represents the total accumulation of FDDs and the y axis shows BSI extent in km^2 at the time. The amount of FDDs is variable year to year which shows up in the difference in length of each line. 27

Figure 13 Estimated ice growth in Elson Lagoon based on the number of FDDs using Lebedev's equation outlined in section 2.5. 28

Figure 14 Seasonal progression of BSI in Elson Lagoon between Nov 18th (dark red) and May 11th (light red). (A) 2017-2018 winter growth season. (B) 2018-2019. (C) 2019-2020. (D) 2020-2021. (Bottom) Quantitative visualization of BSI extent for each year as a product of km^2 (left axis) and percent of total lagoon area covered by BSI (right axis). 29

Figure 15 Seasonal progression of BSI in Simpson Lagoon and Stefansson Sound between Nov 22nd (dark red) and May 3rd (light red). (A) 2017-2018 winter growth season. (B) 2018-2019. (C) 2019-2020. (D) 2020-2021. (Bottom) Quantitative visualization of BSI extent for each year as a product of km² (left axis) and percent of total lagoon area covered by BSI (right axis)..... 30

Figure 16 Seasonal progression of BSI in Kaktovik, Jago and Avery lagoons between Nov 19th (Dark red) and Apr 22nd (Light red). (A) 2017-2018 winter growth season. (B) 2018-2019. (C) 2019-2020. (D) 2020-2021. (Bot) Quantitative visualization of BSI extent for each year as a product of sq km's (left axis) and percent of total lagoon area covered by BSI (right axis)..... 31

Figure 17 Sediment core collected near in Elson Lagoon at ice-sediment core #2 in Figure 5 April 27th, 2021. (a) Total core length is 71 cm, with 53 cm being BBSI and the remaining 18 cm being frozen sediment. (b) Closer view of the center of the ice core, which broke into two pieces upon retrieval above the ice/seafloor interface. Temperature reading line up next to where they were taken in the core. - 9.9°C at the snow/ice interface, -8.6°C at 30 cm down core, -9.3°C at the bottom of the ice core, and air temperature at time of collection was -5.6°C..... 34

Figure 18 UBSI core collected in Elson Lagoon near ice sediment core #1 April 27th, 2021. (a) Total core length is 90 cm (b) Closer view of the bottom of the core. (b) Temperature reading line up next to where they were taken in the core. Temperature was -7.7°C at the bottom of the core, -7.8°C in the frozen sediment, and -8.2°C at the snow/ice interface. 35

Figure 19 Comparison of InSAR detection of BSI and results from drill hole observations at each transect. Values in the rows indicate the number of drill holes identified as either BSI or not BSI using In-SAR based observations and values in the columns represent the number of drill holes which were identified as either BSI, BBSI, UBSI, or floating ice determined using direct in-situ measurements. (*) indicate the addition of the anomalous drill hole observations noted in transects C and D, which were added to the UBSI category for this analysis..... 39

List of tables

Page

Table 1 Breakdown of drill hole observations by water depth..... 21

Table 2 Date at which ice at each hole became bottomfast along with the number of subsequent FDDs after initial contact with the seafloor. The amount of potential ice growth lost due to grounding is shown in column 4, which uses the ice growth estimate equation outlined in section 2.5. The last column shows the range of water depth/ice thickness of the holes at which ice became bottomfast during that period. 37

1 Introduction

The Arctic has undergone rapid changes in the last two decades due to climate change and sea ice extent and coverage has been declining at rates never observed in this region [Perovich *et al.*, 2020]. Models have predicted that the Arctic will see its first ice free summer by the year 2035 [Stroeve *et al.*, 2012] [Docquier and Koenigk, 2021]. As sea ice continues to have a decreased presence in the Arctic, nearshore coastal regions will see significant changes in shallow regions along the coast, including river deltas and lagoon systems. Sea ice adjacent and attached to the coastline is known as landfast ice. Most landfast ice remains floating, but where the water is shallow enough, the entire water column can freeze, forming bottomfast sea ice (BSI). Figure 1 shows how BSI progresses from having a small presence in the shallowest regions during the initial fall freeze up through its maximum extent in mid-winter.

Unlike floating landfast sea ice, which is free to rise and fall with changes in sea level, vertical motion of BSI is eliminated or limited by contact between the bottom and ice and the seafloor. As a result, BSI is the most stable part of the landfast ice and may therefore be well suited for supporting ice roads or other infrastructure. Typically, an active tide crack forms at the boundary between BSI and floating ice, such that new cracks form as BSI extends further into the deeper waters, while older cracks become inactive. Hence, tide cracks can be useful for identifying BSI and delineating its spatial extent. The lateral extent of BSI is primarily controlled by ice thickness and the local bathymetry. In places where the bathymetry slopes gently offshore, such as Arctic lagoons and deltas, BSI can extend for multiple kilometers from the shoreline. This also means that a small reduction in ice thickness can result in significant retreat of BSI extent [Solomon *et al.*, 2008; Stevens *et al.*, 2010].

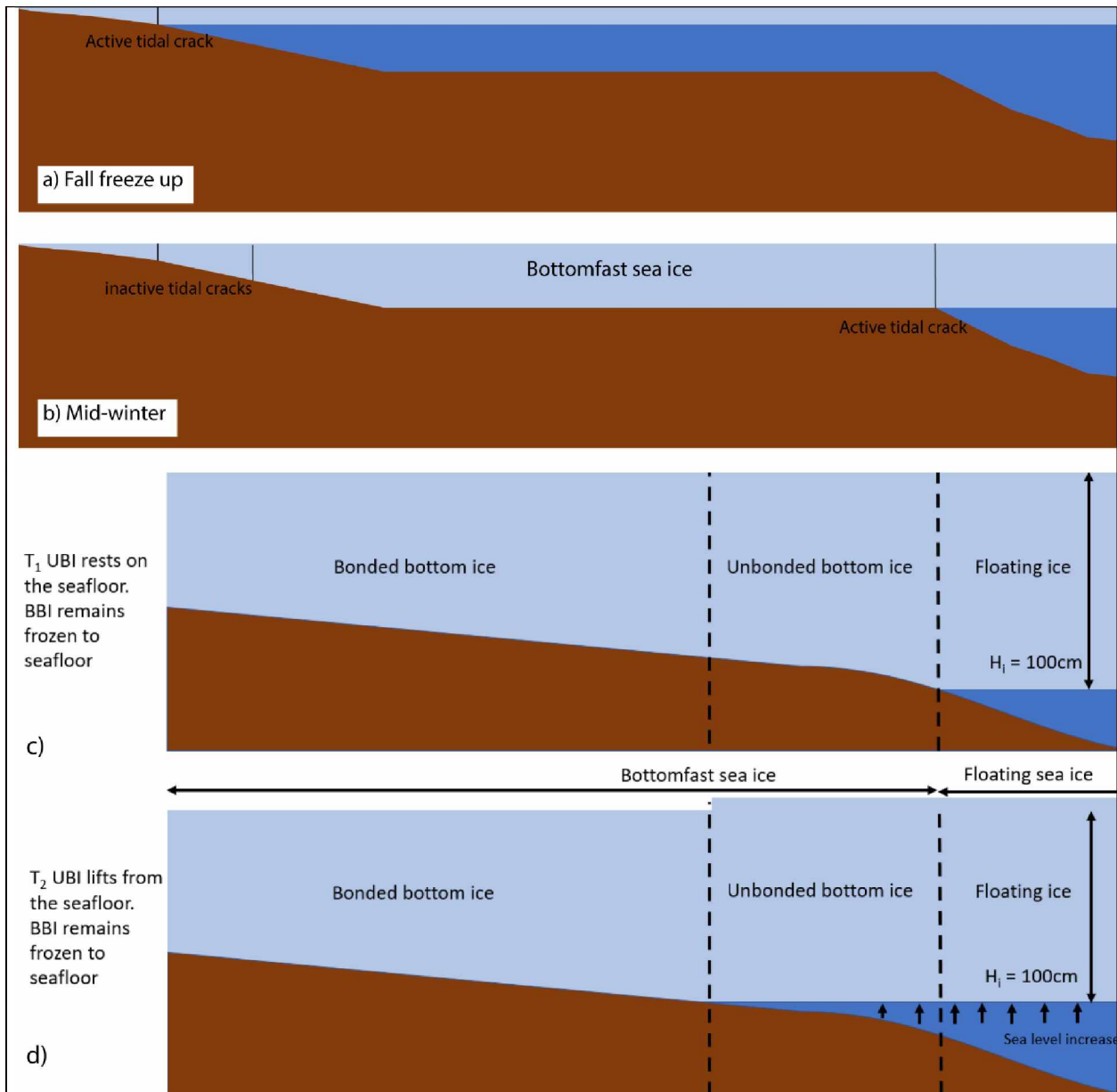


Figure 1. Idealized cross-sections of the bottomfast ice zone at different times of year, and under different sea level states. Sea level can be affected by a number of variables such as changes in tides, strong winds, or winter storm events. a) Early winter with BSI found only in shallowest water and with a single, active tide crack. b) Late-winter with maximum BSI extent and both inactive and active tide cracks. c) A low-water scenario where both BBSI and UBSI are in contact with the seafloor and only the floating sea ice has a layer of sea water beneath it. d) A high-water scenario in which while the BBSI remains securely frozen to the seafloor, but the UBSI has been lifted from the seafloor allowing sea water to circulate beneath. This temporary detachment is what separates BBSI from UBSI and the period when UBSI is in contact with the ground separates UBSI from floating sea ice which always has a layer of sea water beneath it.

Prior research involving BSI has been primarily focused on either its thermal properties in connection with submarine permafrost levels [Osterkamp, 2001; Solomon et al., 2008; Stevens, 2011; Overduin et al., 2016; Angelopoulos et al., 2020] or its lateral extent [Dammann et al., 2018] at the pan Arctic scale. Here, we focus on three shallow lagoon systems along the Alaska coast of the Beaufort Sea, in which BSI is expected to have a direct impact on benthic biota and potentially impacts exchange between the terrestrial and marine systems (Figure 2). At this scale, we investigate the transition between BSI and floating sea ice and the nature of the interface between the sea ice and seafloor.

In defining this transition, we propose it is helpful to consider two types of sea ice within the BSI zone: Bonded bottomfast sea ice (BBSI) is ice that is mechanically attached to the seafloor via a frozen interface. By contrast, unbonded bottomfast sea ice (UBSI) is ice that rests on the seafloor but is not attached. Since UBSI is not mechanically attached to the seafloor, it may be subject to limited vertical ice motion during periods of high water (Fig XX). Similarly, floating ice may temporarily become UBSI if the water level drops sufficiently. High water events can lift UBSI from the seafloor, allowing for additional ice growth and leading to a process referred to as tide jacking whereby the ice surface is left at a higher elevation when the water level subsides. This will also mean that a higher sea level will be required to lift the ice in the future. The process of lifting the ice also allows some flushing of the hypersaline water that accumulates beneath the ice due to salt rejection during the freezing process.

In this thesis we will confirm the distinction between BBSI and UBSI and discuss the importance in understanding how each type of ice affects the underlying thermal regime in the seafloor and different methods of detecting the extent of BSI, BBSI, and UBSI. By appropriately identifying the different types of BSI we can better understand the environmental impacts that come with changes in its extent as well as improving the accuracy of mapping efforts and seasonal monitoring. Additionally, this study attempts to show how these two types of BSI differ in their interactions with submarine permafrost and, more specifically, the active layer (Figure 3). The distribution and depth of the submarine permafrost layer is greatly affected by the extent and duration of BSI during winter. Areas with near-surface submarine permafrost and thin active layer are going to be found in zone 3 in Figure 3 as BSI couples the seafloor sediment with freezing atmosphere temperatures in winter, preventing additional thawing to occur.

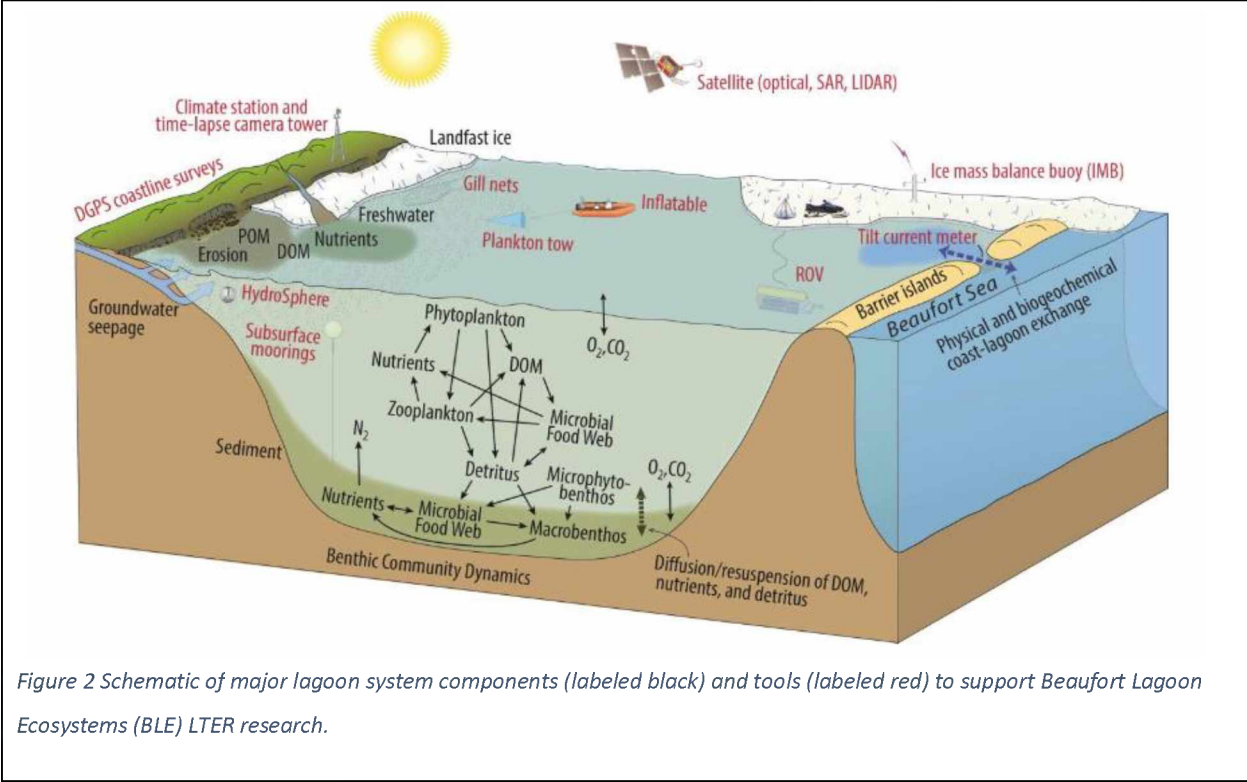
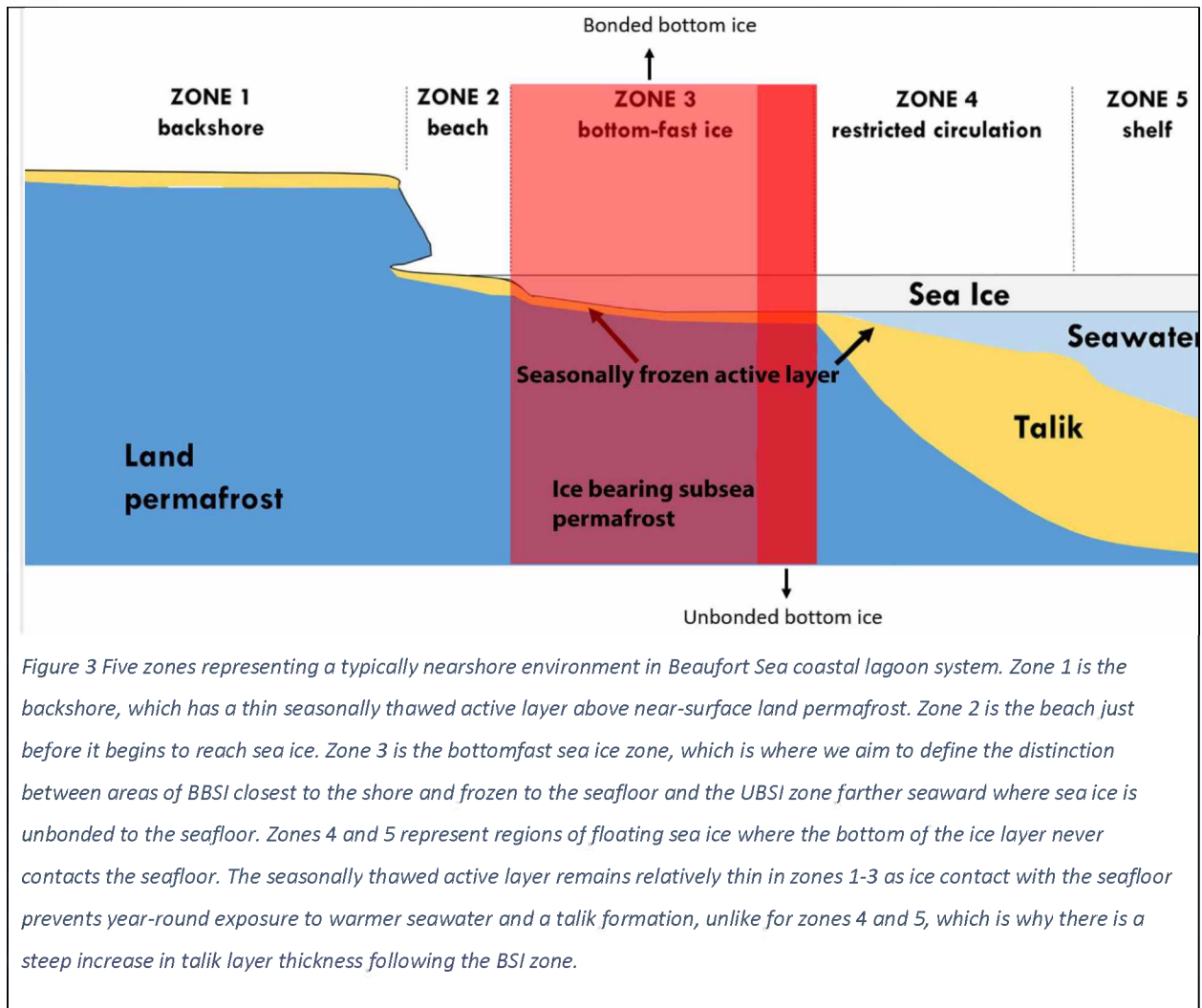


Figure 2 Schematic of major lagoon system components (labeled black) and tools (labeled red) to support Beaufort Lagoon Ecosystems (BLE) LTER research.



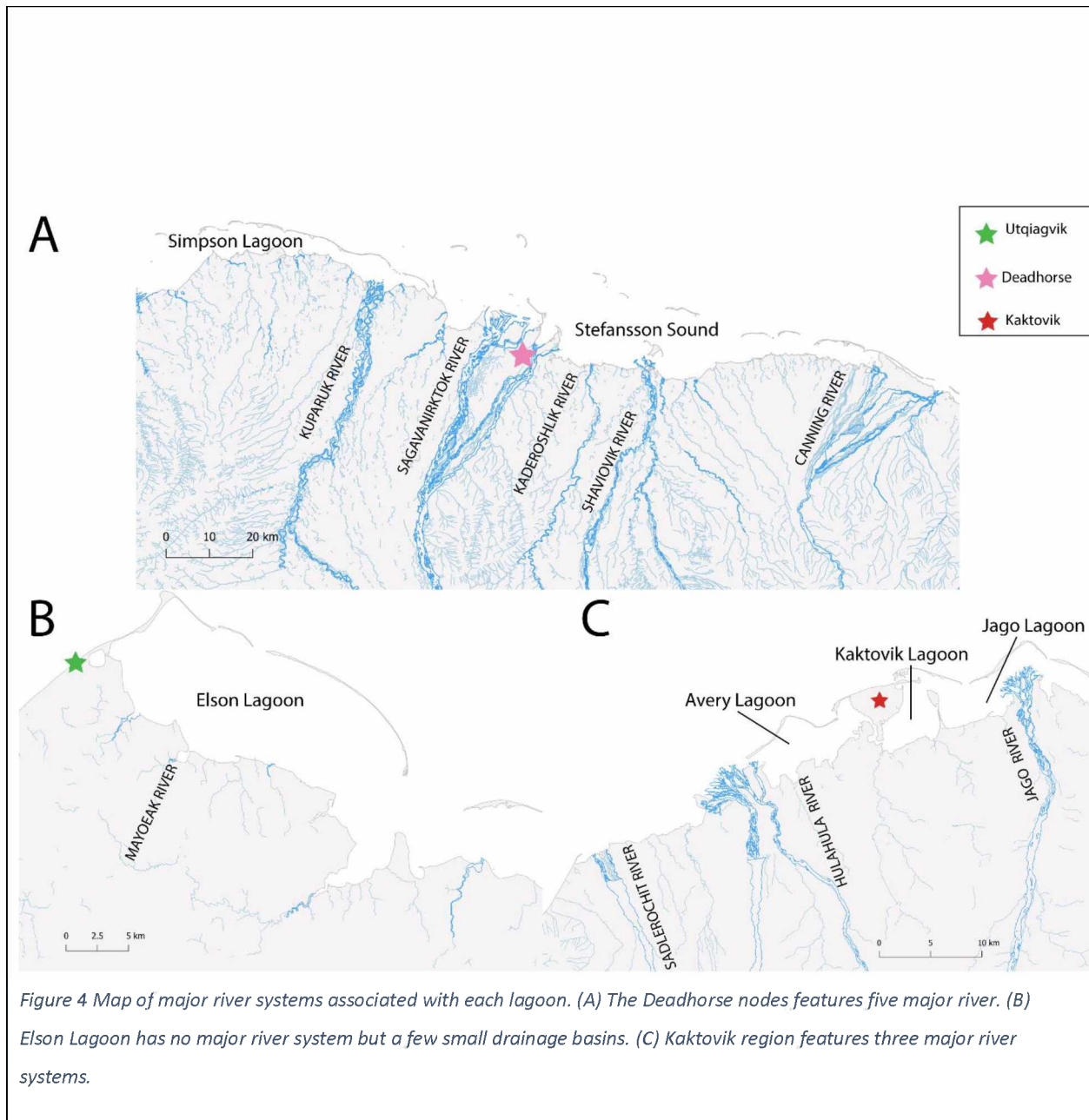
Submarine permafrost is cryotic ($<0\text{ }^{\circ}\text{C}$) sediment and rock overlain by a marine water column [Osterkamp, 2001]. Submarine permafrost is a relic of land-based permafrost that was inundated by the sea and, when compared to permafrost on land, is typically warm and generally degrading [Osterkamp, 2001]. Submarine permafrost traps significant amounts of methane and organic carbon, which could be released to the atmosphere in the event of thawing [Overduin *et al.*, 2015]. The active layer, the seasonally thawed surface layer above permafrost, is located just below the seafloor surface in areas with BSI and freezes during the winter [Solomon *et al.*, 2008]. In the summer months the active layer will increase in thickness as warm lagoon water caps the seafloor until conditions conducive for BSI are met next season [Solomon *et al.*, 2008]. The freezing and thawing process taking place within the sediments can force concentrated brine towards greater depths into seabed sediment, exacerbating future thawing [Overduin *et al.*, 2016]. As seawater freezes to ice it only retains about 30% of the salt

while rejecting the remaining amount through brine channels. The dense brine flows downward and replaces less saline water in the sediments when possible. By understanding where the two types of BSI occur and how they interact with the seafloor we can better predict seafloor and marine life responses to BSI presence and retreat.

2 Methods and Data

2.1 Study regions

Three study sites (A, B, C in figure 4) span a 500 km stretch of coastline along the Alaskan Beaufort Sea, half of which is skirted by irregular and discontinuous barrier islands that enclose numerous shallow lagoons and bays where the water depth is < 7m. This study comprises six of these lagoon ecosystems within three geographic nodes along the coast (Figure 4). This research is in conjunction with a long-term ecological research program in the Beaufort Lagoon ecosystem (BLE-LTER, <https://ble.lternet.edu/>), which focuses on interactions between terrestrial inputs, sea-ice dynamics, and ocean exchange that control lagoon ecosystems along the Arctic Beaufort Sea coast over seasonal to multi-decadal timeframes. Sea ice at these nodes is first-year and predominately smooth ice. These systems vary in terrestrial/freshwater inputs, ocean connectivity, and geomorphology. The western node includes Elson Lagoon, which lies adjacent to the native Inupiat village of Utqiagvik (formerly Barrow). The central node, situated at Deadhorse (Prudhoe Bay), includes Simpson Lagoon and Stefansson Sound. Kaktovik, Jago, and Avery lagoons, adjacent to the native Inupiat village of Kaktovik on Barter Island, compose the eastern node. The eastern node is roughly 187 km² of combined lagoon area and is bounded by discontinuous barrier islands. This node features three major river systems: Jago, Hulahula, and Sadlerochit rivers. The central node is roughly 1725 km² of combined area and hosts five major river systems: Canning, Shavirovik, Kaderoslik, Sagavanirktok, and Kugaruk rivers. The western node consisting of only Elson lagoon with no major river systems covers 329 km² of lagoon area (Figure 4). All validation data were collected at the western node including, *in situ* auger measurements, ice core collection, and conductivity surveys.



2.2 Detecting BSI using SAR interferometry

The ability to distinguish BSI and floating ice using SAR imagery has been well documented within inland lakes where areas with a high contrast in dielectric properties at the ice-water interface have been identified as floating ice [Hallikainen and Winebrenner, 1992]. In salt water environments this method is less effective as the penetration of the SAR signal is reduced caused by the variations of salinity and brine inclusions, which can prevent the detection of the ice-water interface [Hallikainen and Winebrenner, 1992]. The ability to detect the contrast between low-backscatter BSI and high-

backscatter floating sea ice is found to be critically dependent on the roughness of the ice-water interface in addition to the presence of brine inclusions, which enhance forward scattering of the bottom-reflected signal [Eicken *et al.*, 2005]. Instead, Dammann *et al.* [2018] have shown that the lateral extent of BSI can be mapped using SAR interferometry (InSAR), which is a signal processing technique that calculates the phase difference between two complex SAR images acquired with similar viewing geometries [Moreira *et al.*, 2013].

Using images acquired at different times, InSAR can observe cm-scale motion of the ice surface, which results in variations in the interferometric phase. Floating landfast sea ice rises and falls with changes in sea level, but BSI is not free to move vertically due to its contact with the seafloor. Hence, using InSAR, BSI can be distinguished from floating sea ice by a lack of variation in interferometric phase. Dammann *et al.* [2018] demonstrated this technique at a pan-Arctic scale, while Tibbles *et al.* [2018] used InSAR to identify floating ice extent and overwinter habitats for whitefish on a smaller scale of Arctic lagoons.

Here, we use the InSAR methodology developed by Dammann *et al.* [2018] to map the lateral extent of BSI in three coastal lagoon systems along the Alaska Beaufort Sea coast from December 23rd, 2017 to April 30th, 2021. We acquired complex interferometric wide (IW) mode SAR data from Sentinel 1, which is a constellation of two C-band SAR systems (S1-A and S1-B), each on a repeat orbit interval of 12 days. Both satellites share the same orbital plane with a 180-degree phase offset, which allows for 6-day periods between acquisitions from either satellite. All SAR data were ordered and interferometrically processed through the Alaska Satellite Facility's online engine HYP3, uses GAMMA algorithms to produce the differential InSAR images [Hogenson *et al.*, 2016]. All SAR images were multi-looked with a 10x1 scheme which averages 10 pixels in range direction (2.7) and 1 pixel along track direction yielding approximately 2.7 x 22.5 m of spatial resolution and pixel size of 40 x 40 m.

In an interferogram, the absolute phase value of an individual pixel does not provide useful information, but a phase difference between pixels indicates relative motion. Any difference in line-of-sight surface displacement between two acquisitions will result in an interferometric phase difference, $\Delta\phi_{disp}$, given by:

$$\Delta\phi_{disp} = \frac{4\pi\Delta LOS}{\lambda}$$

where ΔLOS is displacement in the line-of-sight direction and λ is wavelength.

In the case of Sentinel 1 C-band SAR with a wavelength of 5.55 cm, a phase variation of 2π corresponds to a ΔLOS of 2.78 cm. Phase values are wrapped within the interval $0-2\pi$ and so continuous variations in surface displacement greater than 2.78 cm will lead to “fringes” in an interferogram. The presence of fringes is indicative of relative displacement of the ice surface while an absence of fringes indicates regions of relative stability. Although Dammann [2016] demonstrated the possibility of using an inverse approach to estimating the 2-dimensional strain based on the patterns of these fringes, we limited our analysis here to the use of InSAR to distinguish between the presence or absence of ice surface motion.

Following Dammann et al. [2018], we identified BSI based on a maximum phase variation from the coastline of 0.9 radians, corresponding to less than 1.5 cm of relative motion between the ice and land. Seaward BSI boundaries were hand drawn in QGIS (Quantum Geographic Information System software version 3.10.2) based on visual inspection of each interferogram. BSI extent was mapped by hand in QGIS using the polygon tool and saved as individual shape files for each interferogram. The seaward extent of BSI was traced along the identified boundary and the landward side of the polygon was created well within the coastline to allow a difference to be created by overlaying the coastline file with the polygon.

2.3 Detecting BSI using electromagnetic (EM) sounding

As an additional means of detecting the boundary between BSI and floating ice, we used an EMP400 electromagnetic (EM) profiler manufactured by GSSI to measure the apparent conductivity (σ_a) of the ice and seafloor beneath the instrument and any seawater in between. The EMP400 emits a primary EM field at up to three different frequencies between 1 and 16 kHz. The instrument then measures the in-phase (I) and quadrature (Q) components of the secondary field induced in the subsurface. σ_a is proportional to Q and is calculated automatically based on the fixed spacing of transmitter and receiver coils. Since the conductivity of sea ice and the seafloor of the lagoon is low compared with that of seawater, the measured value of σ_a is sensitive to the presence of seawater below the ice and the distance to the ice-water interface. In typical sea ice applications, EM profiling takes advantage of this sensitivity to measure the thickness of the sea ice [Haas et al., 1997]. Here, we are primarily interested in distinguishing BSI from floating ice, so we chose to operate the EMP400 at its highest frequency (16 kHz). This minimizes the penetration of the EM field into the seawater, thereby maximizing the sensitivity of σ_a to the presence of a thin layer of seawater.

The EMP400 was mounted on a plastic sled and pulled behind a snow machine and operating in the horizontal dipole mode, i.e., with the coil planes aligned vertically. The data logger for the EMP400 is equipped with a global position system (GPS) device and was configured to record, I , Q , and σ_a together with the latitude and longitude of each measurement every 0.5s. The EM-sled was towed in a zig-zagging path across the southern shoreline of Elson Lagoon and a shoal of shallow water BSI was expected to be found. A total of three surveys were carried out in late April 2021. Operation of the EMP400 allows the instrument to be calibrated in the field to account for the height of the antenna above the ground and the presence and location of nearby conductive materials, such as the data logger and metal components of the sled. Unfortunately, the calibration settings were inadvertently reset between surveys, resulting in fixed offsets between conductivity measurements from different surveys, and some negative conductivity values. To correct for this, we identified cross-over points where the same location was visited on multiple surveys. Using measurements from these locations, we computed a mean offset correction between surveys. We also applied an additional offset such that the minimum value of σ_a on any survey was zero.

2.4 Drill hole observations

2.4.1 Drill hole strategy

Four transects across the BSI transition boundary were identified based on inspection of contemporary interferogram images between April 24th and May 3rd, 2021. Along each of the four transects, we drilled through the ice using Kovacs augers (5-cm in diameter) for direct ice thickness measurements, to verify the presence or absence of water beneath the ice and determine the frozen or unfrozen state of the seafloor. Auger holes were drilled through the ice. In the case of BSI (dry hole), auguring was ceased once sediment had been reached. As this method relies on the user's ability to feel when they have reached the bottom of the ice, drilling was done in small 1-2 cm intervals. While there is room for error as the drill can dig into the sediment upon reaching the bottom, this method reduces the scale of error to a few centimeters. Auger holes that were drilled through floating ice filled with water once the bottom of the ice was reached. On each transect, we concentrated auger holes in the vicinity of the seaward boundary of BSI to identify the transition more precisely between BSI and floating sea ice. At each hole we measured snow depth, ice thickness, water depth, salinity, conductivity, and water temperature and noted whether the interface between the ice and sediment was wet, dry, or slushy (see below). Additionally, we determined BSI was bonded to the seafloor (BBSI) if the drill hole remained

dry after the auger had passed into the frozen seafloor. If the hole filled with water, we determined that the BSI was unbonded (UBSI). Underneath UBSI, we found that the seafloor could be frozen or unfrozen.

2.4.2 Snow depth

Snow depth was measured once directly next to auger hole's locations using a snow probe with an error of +/- 0.5 cm. The snow probe was inserted into the undisturbed snow until it reached the top of the ice layer and measurements were taken from the top of the ice to the top of the snow layer.

2.4.3 Ice thickness

Where the ice was floating, we measured ice thickness using a Kovacs Enterprise ice thickness gauge, which consists of reinforced tape measure with a hinged bar at the end. The hinge is opened, and the bar is lowered through a hole in the ice until it is beneath the ice bottom. Provided there is enough space below the ice for the bar to completely clear the hole (approximately 5 cm), it will then catch on the bottom of the ice hole when the tape is gently pulled up. The thickness of the ice can thus be measured with an accuracy of +/- 0.5 cm. In areas where the ice was floating but the distance between the bottom of the ice and the seafloor was less than approximately 5 cm, this gauge did not work. Instead, we used a steel tape measure, which required delicately hooking the small tab at the zero-point on the edge the hole. Since the bottom of the hole did not always have a well-defined edge, we estimate our accuracy was no better than +/- 1.0 cm. Where the ice was in contact with the seafloor, we measured the ice thickness using the snow-depth probe for ice < 1.2 m thick and the steel tape measure for ice > 1.2 m. In both cases, the accuracy of the measurements relied on our ability to stop drilling at the bottom of the ice before going into the sediment and we, therefore, estimate an uncertainty of +/- 2.0 cm.

2.4.4 Water depth

Water depth was measured by using the Kovacs ice thickness gauge. By lowering the bar until laid flat on the seafloor, the water depth was measured according to the position of the water on the tape measure. The thickness of the water layer beneath the ice was calculated by the difference between the distance from the top of the ice to the seafloor and ice thickness.

2.4.5 Interface characteristics

Holes that were identified as "wet" were holes with enough water to use a YSI Pro30 salinometer to collect salinity, conductivity, and water temperature readings. This was not always applicable in all

“wet” holes as some areas had restricted water flow beneath the ice, disallowing the hole to recharge with enough water to collect a reading. The salinometer could not be used for holes identified as “slushy” either as the space between the bottom of the ice and the seafloor consisted of ice that was not completely frozen or liquid. We also noted whether the sediment immediately below the ice was frozen or not by probing the sediment surface once the hole was drilled and feeling for a solid frozen surface or an unfrozen surface, which the probe could penetrate.

2.5 Ice and sediment coring

At five locations adjacent to auger holes where the ice was in contact with the seafloor, we recovered ice and sediment cores using a Snow, Ice, and Permafrost Research Establishment (SIPRE) corer equipped with tungsten carbide cutters. The SIPRE corer allowed us to extract a 7-cm diameter core extending from the top of the sea ice to approximately 30 cm into the sediment below. Unlike in floating ice, these core holes were either dry or became only partially filled with seawater. Together with the higher density of sediment-laden ice and frozen sediment, BSI core sections did not float to the top of the hole. We, therefore, used a core retrieval device consisting of a 10-cm diameter PVC tube that fit down the hole around any core sections sitting on the bottom. A bent steel tab at the bottom of the tube prevented the core section sliding out when the tube was lifted out of the hole. Using this technique, we were able to recover the full ice-sediment core even if it broke into sections during drilling or if the ice was not bonded to the seafloor. This allowed us to directly inspect the interface between sea ice and sediment upon retrieval.

Immediately after extraction, we measured temperature at 10 cm intervals throughout the ice column, at the ice sediment interface and within the sediment below. To measure temperature at each location, we drilled a roughly 2 mm diameter hole to the mid-point of the core and inserted a Traceable 4502 long stem digital thermometer, which has a stated precision of 0.1 °C above -20°C. Each core was then cut into 5 cm sections, each of which was stored in a resealable plastic bag for transport back to land. Ice core sections were then melted and the salinity of the melted sample (i.e. bulk salinity of the ice) was measured using a YSI Pro30 conductivity meter. The sediment cores were thawed inside a rigid watertight container and allowed to settle so that we could obtain a measurement of the salinity of the pore water. Since salinity of the pore water was found to be outside the limits of the conductivity meter, we diluted with a known volume of distilled water until the salinity was within range.

2.6 Freezing degree days

Accumulated freezing and thawing degree days were calculated using air temperature data measured by automated weather stations at the nearest airport to each lagoon. For Elson Lagoon, we used data from a station at the Barrow Wiley Post-Will Rogers Memorial Airport in Utqiagvik (WBAN: 27502). For Simpson Lagoon and Stefansson Sound, we used data from the station at Deadhorse airport (WBAN: 27406). For Kaktovik and Jago lagoons, we used data from the Barter Island airport at Kaktovik (WBAN: 27401). All data were downloaded from the National Climate Data Center (NCDC) at <https://www.ncdc.noaa.gov/cdo-web/>. Freezing degree days (FDDs) were calculated by summing the daily mean air temperatures of days with mean temperature below 0 °C since the onset of freezing. We defined the date of the onset of freezing as being the first day with an average temperature below 0 °C that was also the first day of a 7-day period that had an average temperature below 0 °C [Mahoney *et al.*, 2007].

Additionally, by using air temperature data from the respective airport weather stations, it is possible to use FDD to estimate the earliest date when ice formation may have started for each year. Once the average daily air temperature is below freezing for seven days in a row, we can start accumulating FDDs. With the number of FDD's monitored for each lagoon each year we can identify how many FDDs have occurred after the earliest observable BSI formation identified from interferograms. Ice thickness (H) can also be estimated using a simple calculation based on an equation from Lebedev (1938) derived from the cumulative number of FDD (θ).

$$H = 1.33\theta^{0.58}$$

3 Results

3.1 Transect data

3.1.1 Overview of transects in Elson Lagoon

Drill-hole observations and EM conductivity measurements were carried out along four transects in western Elson Lagoon (Figure 5). Transect A crossed the shallow shoal extending from Tekegakrok Point east to west for approximately 1800 m. Transect B crossed the same shallow shoal in an east to west orientation for approximately 2000 m. Transect C began at the coast and extended approximately 950 m seaward perpendicular to the coastline. Transect D began at the coast and extended approximately 1300 m in the lagoon crossing the Mayoek River drainage basin south of Transect C. In-situ and InSAR-

derived data along each of these transects are shown in Figures 6 – 9. The following subsections describe each type of measurement and observation along each transect.

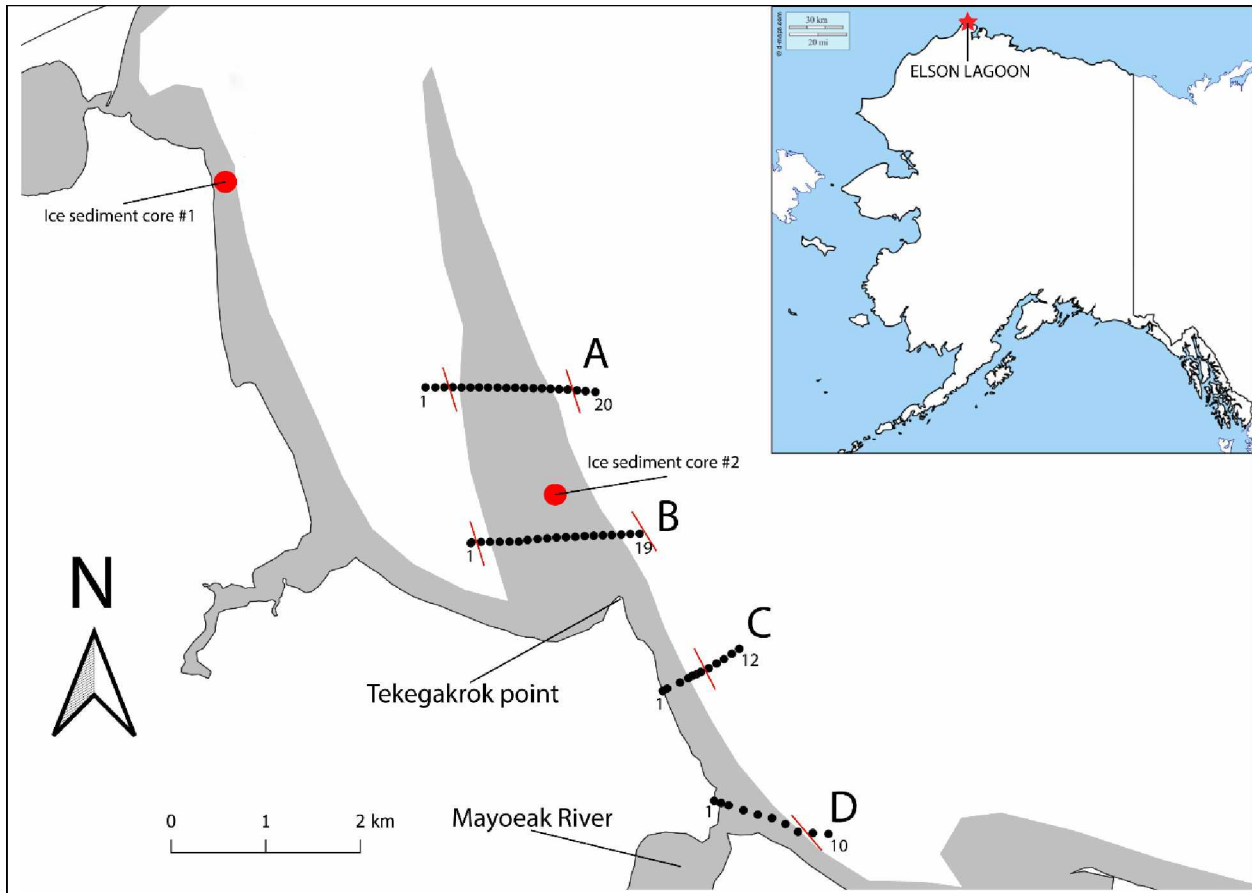


Figure 5 Auger hole transect locations relative to BSI extent as determined by InSAR in grey and red hash marks identifying the boundary between BSI and floating ice determined by drill hole observations. BSI extent was identified from interferograms collected between Apr 30th 2021 and May 12th 2021. Location of sediment core collection is marked with a red dot. Grey shaded region represents BSI extent at the time of collection. Sediment core #1 was collected April 24th, 2021, and sediment core #2 was collected April 25th, 2021.

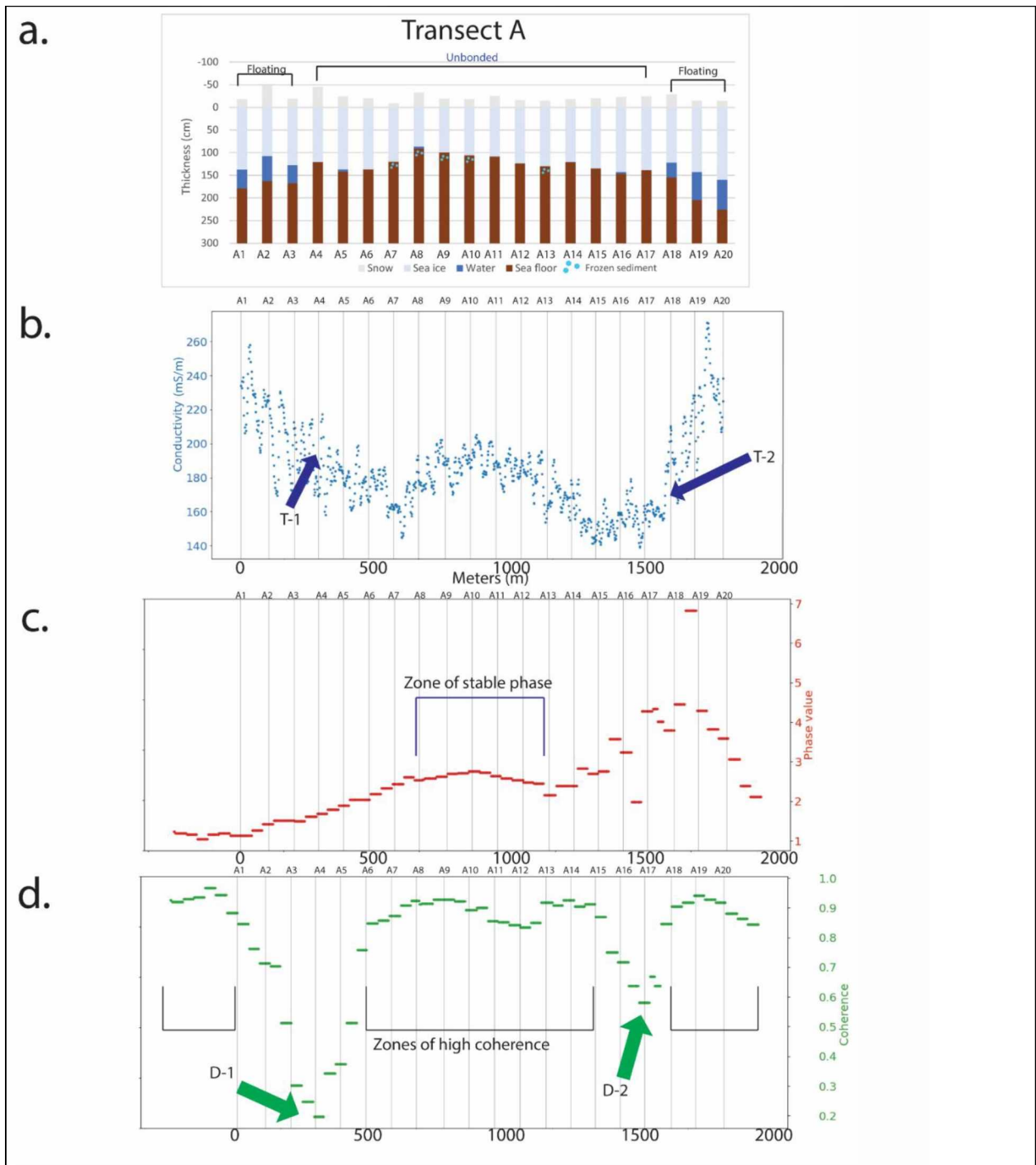
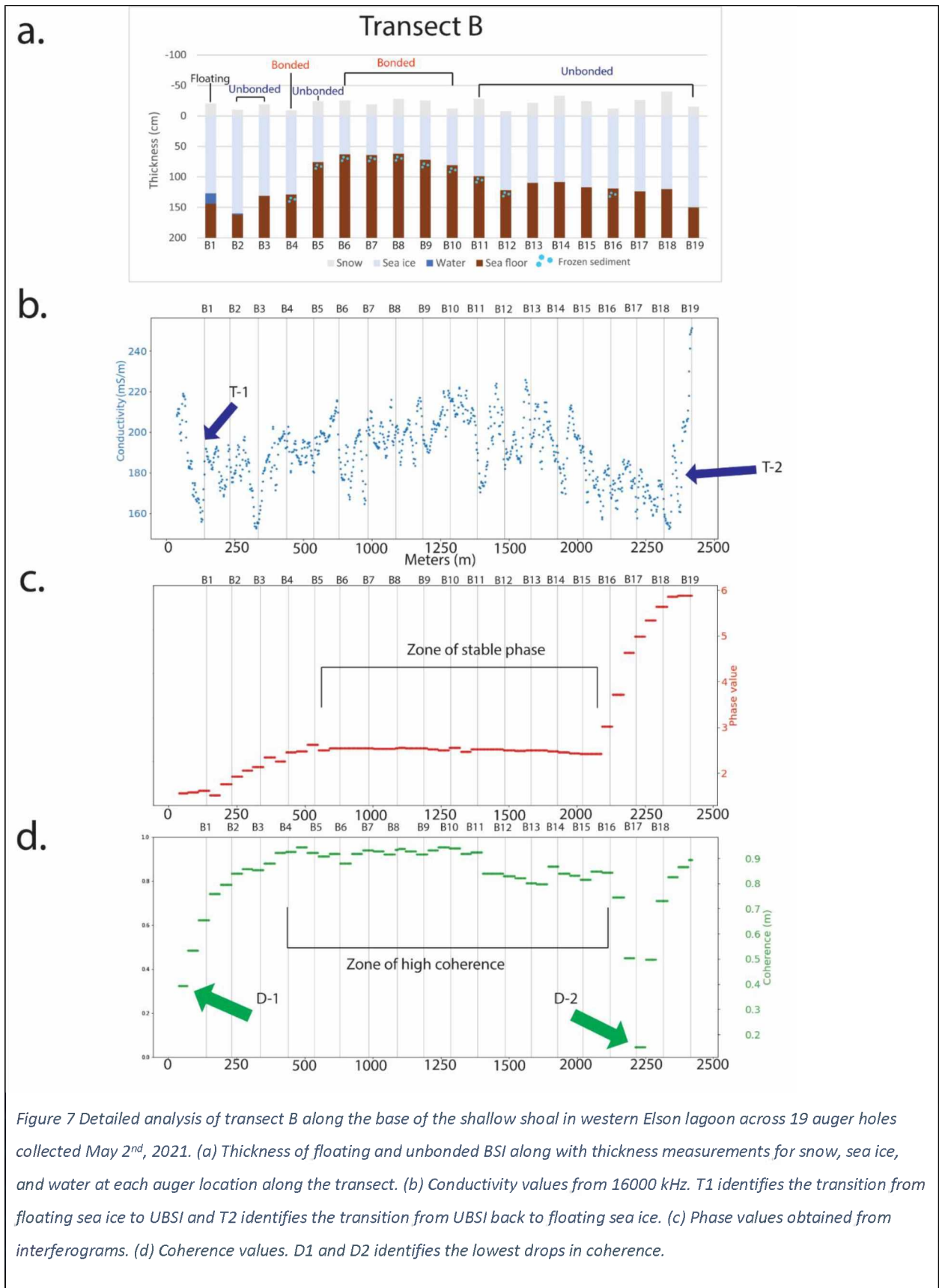
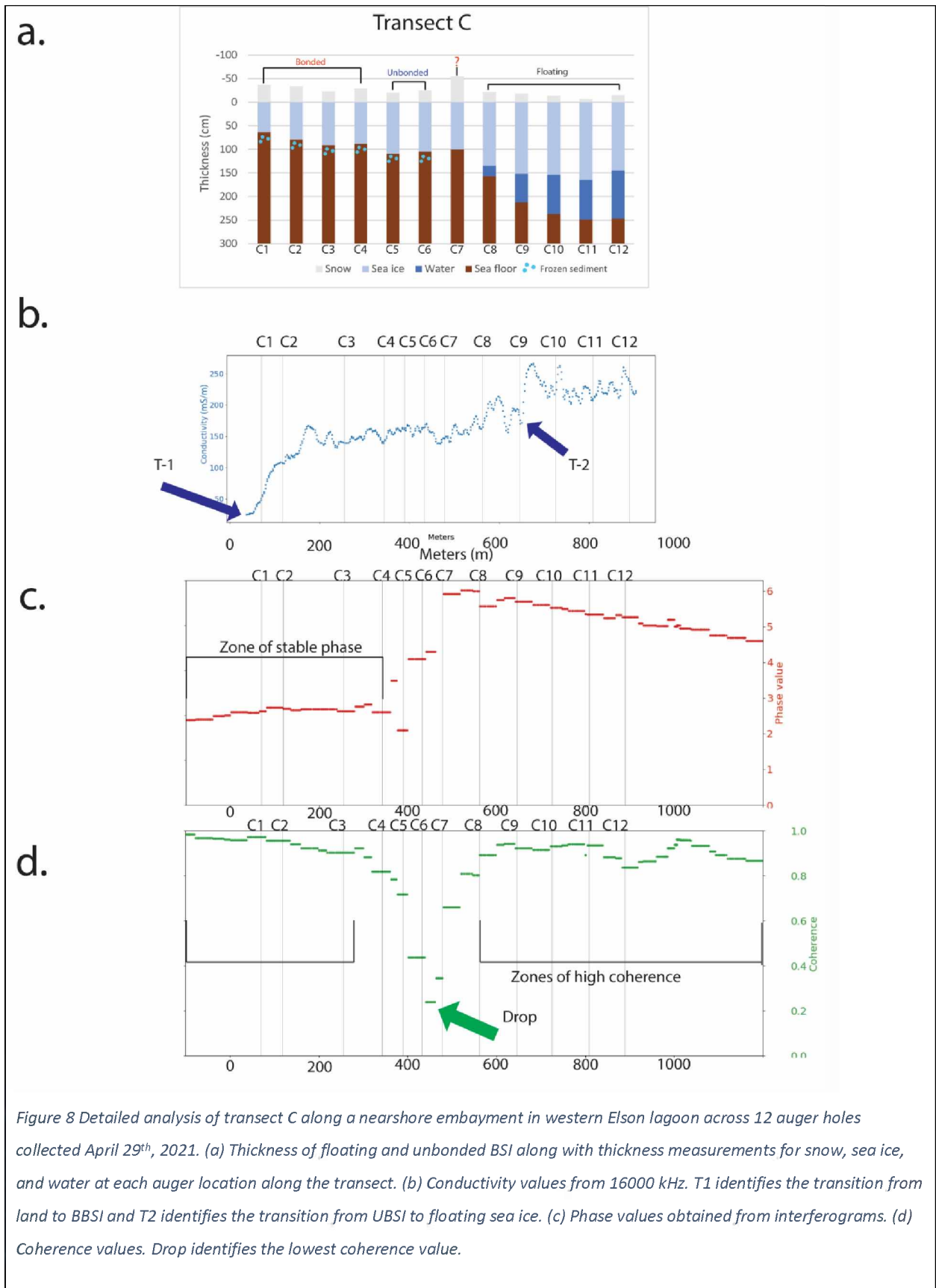
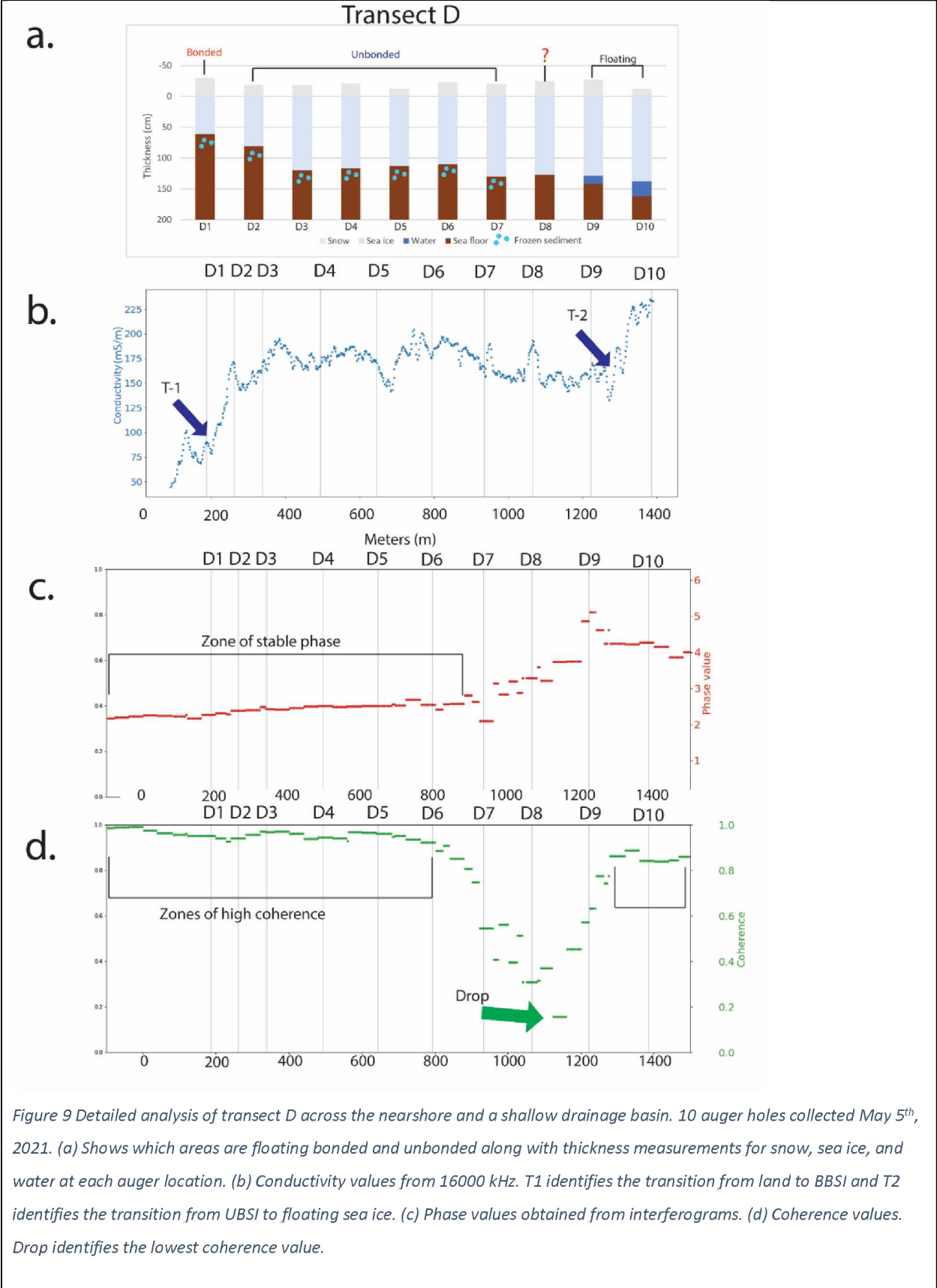


Figure 6 Detailed analysis of transect A along the middle of the shallow shoal in western Elson lagoon across 20 auger holes collected May 1st, 2021. (a) Thickness of floating and unbonded BSI along with thickness measurements for snow, sea ice, and water at each auger location along the transect. (b) Conductivity values from 16000 kHz. T1 identifies the transition from floating sea ice to UBSI and T2 identifies the transition from UBSI back to floating sea ice. (c) Phase values obtained from interferograms. (d) Coherence values. D1 and D2 identify the lowest drops in coherence.







3.1.2 Drill-hole data

Drill hole observations allowed us to identify the transition between BSI and floating ice based on the presence of a measurable layer of seawater between the ice bottom and seafloor. For example, Figure 6a represents data from transect A, which crossed the northern region of the shallow shoal shown in Figure 5 and had floating ice at both ends. At the center of the transect, we found a continuous zone of UBBSI. The transitions from floating ice to BSI and back again occurred between holes A3 and A4 and holes A17 and A18. Overall, ice thickness along Transect A ranged from 0.9 m to 1.6 m (Figure 6a). No BBSI was found across this transect but the shallowest regions in the center of the transect still had frozen sediment at the seafloor between holes A7 and A10 along with hole A13.

Ice thickness measured along Transect B (Figure 7a) ranged between 0.6 and 1.6 m across the transect. There was a transition from floating sea ice to BSI between holes B1 and B2 at the western end of the transect, but the transect did not extend far enough to identify the transition back to floating ice at the eastern end. Between holes B6 and B10, where the bathymetry was shallowest and ice thickness was less than 0.81 m, we found a continuous zone of BBSI. On either side of this region, with the exception of hole B4, the ice was found to be UBSI with either frozen or unfrozen seafloor beneath. Most of the frozen seafloor beneath UBSI was found adjacent to BBSI, but we also found an isolated example of UBSI on top of frozen seafloor at hole B16.

Transect C which began at the coast and extended seaward to deeper waters. Measured ice thickness ranged between 0.6 and 1.6 m along this transect. The holes where sea ice was 1 m or less were found to be BBSI, including the first four holes extending from the coast and again at hole C7 (Figure 8a). The UBSI zone between these bonded ice regions had a thin water layer of less than 5 cm between the ice bottom and frozen seafloor interface. The last five drill holes along this transect, which increased in depth seaward of the coast, were characterized as floating sea ice zone.

Transect D extended from the coast and crossed a shallow region of BSI at the mouth of the small drainage of the Mayoek River and ended at floating sea ice (Figure 9a). Ten drill holes were measured along this transect and ice thickness ranged between 0.6 and 1.4 m. Drill hole D1 encountered BBSI, and the next six holes (D2-D7) found UBSI over a frozen seafloor. Hole D8 was anomalous in that it remained dry after drilling (typically indicating the presence of BBSI), but the sediment at the interface was unfrozen. We were, therefore, uncertain whether to assign this as BBSI or UBSI. If the ice at hole D8 was

bonded, then it would represent the only instance where we found a transition from BBSI to floating ice, since holes D9 and D10 were both identified as floating ice.

Of the 14 drill holes where the water depth was less than 1 m, we found BBSI at 10 holes (71%) and UBSI at the remaining four holes (29%). Twenty-three holes were in water depths between 1 - 1.25 m, and we found that 20 of them (96%) were identified as UBSI while only one (4%) was BBSI. Of the 10 holes at depths between 1.25- 1.5 m, two (20%) were found to be BBSI, while the other eight (80%) were identified as UBSI. All holes at greater depth than 1.5 m were found to be UBSI (Table 1).

Water depth (m)	Total drill holes	# BBSI holes	# UBSI holes	# Floating ice holes
<1	14	10	4	0
1 – 1.25	23	1	20	2
1.25 – 1.5	18	2	8	8
>1.5	6	0	2	4

Table 1 Breakdown of drill hole observations by water depth.

3.1.3 EM conductivity data along transects

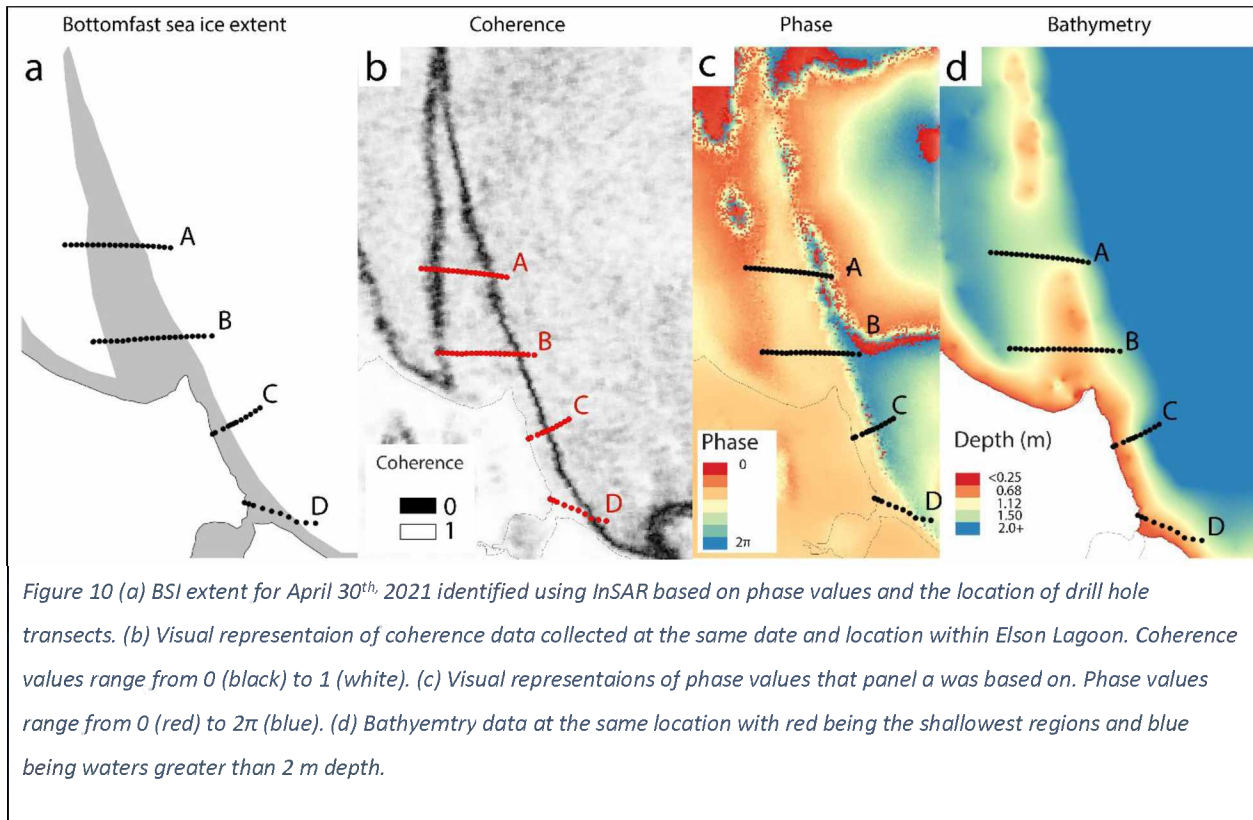
Conductivity measurements were taken using the EMP400, which was pulled behind a snow mobile along all four transects. Each drill hole location was identified by a flag marker and the EMP400 was dragged over the exact location to create the transect. Conductivity differences between transitions from the coast to BSI and then to floating sea ice range from 50 -100 mS/m and smaller variations within the same ice type range between 0-50 mS/m. While there were small scale fluctuations in the BSI regions there did not seem to be a consistent difference in conductivity between BBSI and UBSI. These minor fluctuations occurred at a length scale of approximately 100 m and could, therefore, be explained by the variability of snow depth on top of the ice. As the sled carrying the sensor passes over a snow dune, the distance between the sensor and the bottom of ice increases, leading to a reduction in apparent conductivity.

In each of the transects, the transition from BSI to floating sea ice could be readily identified by abrupt increases in conductivity. Conductivity also consistently increased in areas of floating sea ice as the layer of sea water between the ice and the seafloor increased in thickness with distance from shore. Transect A (Figure 6b) transitioned from floating ice to UBSI between holes A3 and A4, which coincided with a drop in conductivity, labeled T1, due to the absence of saltwater between the ice and the seafloor. Additionally, the inverse pattern occurred at the end of the transect at T2 where the conductivity began

to rise again when saltwater started to be present beneath the ice. Conductivity values in transect B (Figure 7b) remained relatively consistent with a small-scale increase at the center within the BSI zone and a spike on each end of the transect as ice transitions between BBSI and floating sea ice. Conductivity values for transect C steadily increase with distance from the coast (Figure 8b) with the largest increase in conductivity occurring at T1 where we see the transition from land to BBSI and again at T2 at the transition from UBSI to floating sea ice. Transect D (Figure 9b) was a nearshore progression from the coast into the BSI zone (T1) then into floating ice (T2).

3.1.4 InSAR data along transects

InSAR phase and coherence values were extracted along each transect using the GPS-derived locations acquired from the EMP400 (Figures 6-9 c and d). Phase values within areas of BSI were relatively consistent with small variations <1 radian while the transitions between BSI and floating ice were associated with phase value changes of around 3-4 radians. Minor phase fluctuations outside of the BSI region were found to consistently increase or decrease in accordance with the scale of motion between SAR images. Coherence values remained consistently high (0.8 – 1.0 both outside and inside the BSI zone) but dropped to near 0 at the boundary of BSI and floating ice. The decrease in coherence to its lowest point and its subsequent return occurred gradually over the span of 300 – 500 m along each transect.



The phase values for transect A (Figure 6c) increased steadily between holes A1 and A8, meaning that ice at these locations was subject to some surface motion. Between holes A1 and A3, drill hole data confirmed these to be floating ice while holes A4 through A8 were found to be UBSI that experienced some surface motion masking the transition between floating and BSI. Stable phase occurred between holes A8 and A13 as this region did not experience motion at the surface. Following hole A13 there was an increase in phase until hole A17, corresponding to surface motion in one direction and then a decrease in phase, indicating motion of a different direction. Between holes A13 and A17 drill holes confirmed the region to be UBSI, which had some surface motion. The transition from UBSI to floating ice occurred at hole A18, and the rest of the holes to the east were all floating ice. Coherence values (Figure 6d) at this transect appeared to be the lowest at the transition from floating sea ice to unbonded sea ice, holes A4 and A17. In this case coherence was able to detect the boundary between floating and BSI more accurately than by measuring phase alone. Drops in coherence also aligned closely with changes in conductivity at holes A4 and A17 (Figure 6b) while remaining consistent for holes between these two boundaries.

Along transect B, there was an initial increase of phase between hole B1 and B3, corresponding to a transition from floating sea ice at B1 to an USBI region at B2 and B3, which experienced some motion. Phase remained relatively constant between holes B4 and B16 (Figure 7c), identifying this as an area of ice with little or no surface motion. The ice at hole B4 and between B6 and B10 was identified as BBSI. Ice at hole B5 and between B11 and B16 correspond to a region of USBI, which did not show relative motion similar to ice in the BBSI region. Following hole B16, there was an abrupt increase in phase, meaning that the ice surface after this hole moved relative to the ice at the center of the shoal. Coherence values along this transect (Figure 7d) were at their lowest just prior to the first hole B1 and then again at hole B17. This gives a more accurate view of the measured BSI location based on auger hole observations; however, the last two holes (B18, B19) which were found to be USBI during in-situ measurements had high coherence values.

Along transect C, phase values remained relatively constant between holes C1 and C4 (Figure 6c), identifying this as an area of ice with little or no surface motion. The ice at these holes was identified as BBSI. Between holes C5 and C7, corresponding to a region of USBI, there was an abrupt increase in phase, meaning that ice surface between these holes moved relative to the ice closer to shore. Seaward of hole C7, the phase decreased, indicating relative motion of a different nature, and corresponding to floating ice, the nature of which was beyond the scope of this paper. Here, we only consider the presence or absence of ice motion. We also note that the region of increasing phase aligned with the zone of USBI, coinciding with a significant drop in coherence (Figure 8d).

Phase values for transect D (Figure 9c) remained consistent from hole D1 through D7 as there was no surface motion detected in this region. Drill hole observations identified hole D1 to be BBSI and D2 through D7 to be USBI. Phase increased at hole D8 through the end of the transect at D10. Hole D8 was anomalous as a dry hole that was not bonded to the seafloor, and the increase in phase following hole D7 confirmed there was surface motion in this area. Therefore, the transition from BSI to floating ice happened eastward of hole D8 but due to the unique nature of hole D8 we cannot define the transition as USBI to floating or BBSI to floating ice. Coherence values (Figure 9d) dropped the most between holes D8 and D9, which was just prior to when there was an increase in conductivity between holes D9 and D10 (Figure 9b).

3.2 Seasonal progression and interannual variability of BSI extent

3.2.1 Overview of InSAR-derived BSI extent

Having confirmed that discontinuities in interferometric phase near the coastline were commonly related to the transition between BSI and floating ice, we now present an analysis of BSI lateral extent throughout our study region from 2017 to 2021 based on InSAR analysis. A total of 114 interferograms were interpreted to identify the lateral extent of BSI across the three lagoon systems over the four-year period. BSI's lateral extent is represented in square kilometers and as a percent of total area for each study site. Figure 11 delineates the boundary of each lagoon in order to quantify the percent of BSI extent across the total area for each lagoon respectively. The first observation of BSI in the season was variable from year to year at each node, ranging as little as 4% and as much as 10% of the total lagoon area (Figure 12). Year-to-year variations for each node could be seen most prominently in the middle of the growth cycle with the largest differences being as high as 20% of total lagoon area; however, most years' maximum extent remained within 10% of total lagoon area for each node. This is to be expected as BSI formation is primarily dependent on the amount of ice grown during that season and seafloor bathymetry, which is subject to yearly variability depending on the timing and severity of freezing conditions. We calculated the accumulation of FDDs for each node (Figure 12) using the equation outlined in section 2.5; additionally, ice thickness for Elson Lagoon was estimated based on the number of FDDs that occurred in the 2020-2021 winter season (Figure 13) based on Lebedev's equation also outlined in section 2.5.

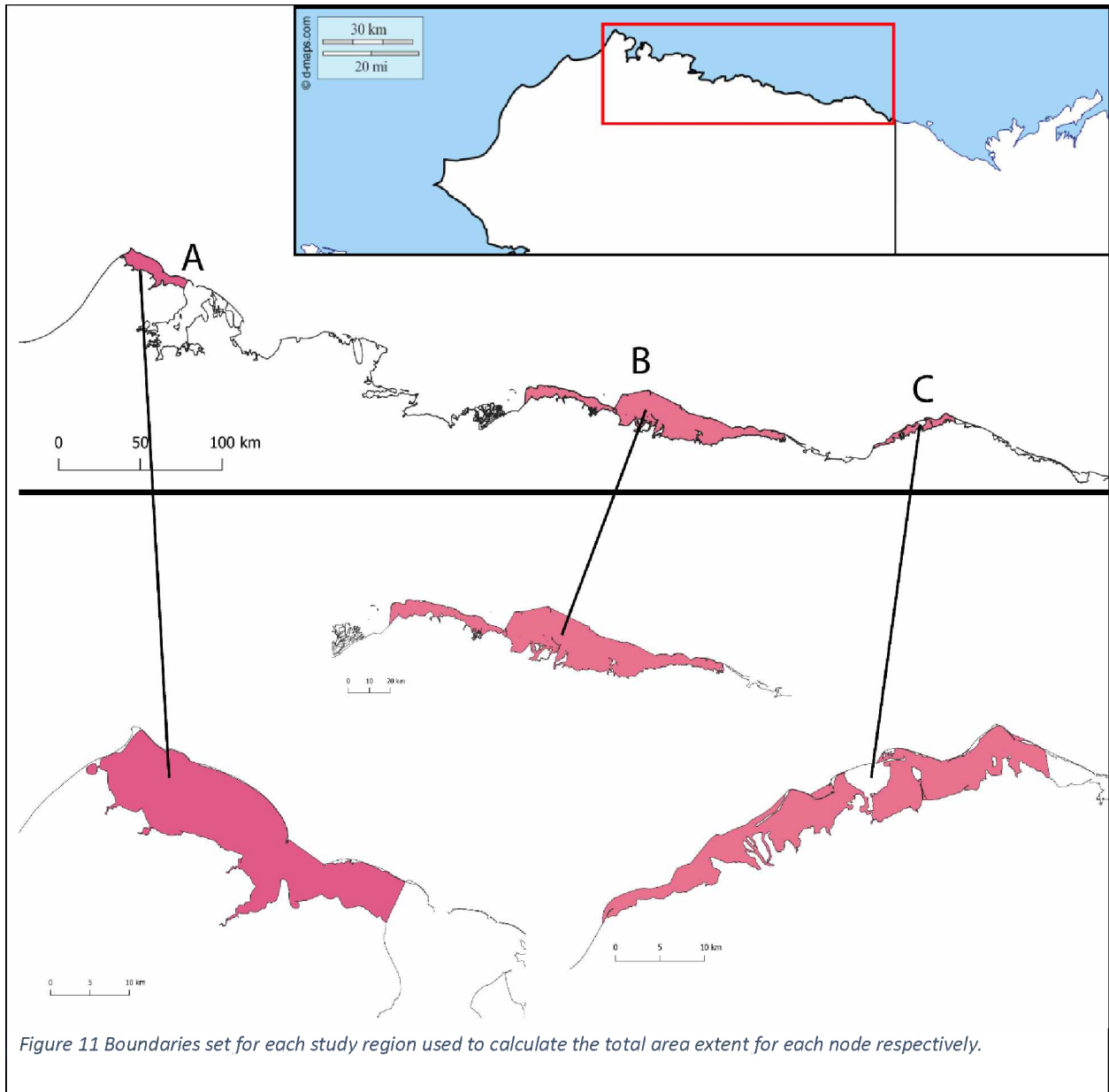


Figure 11 Boundaries set for each study region used to calculate the total area extent for each node respectively.

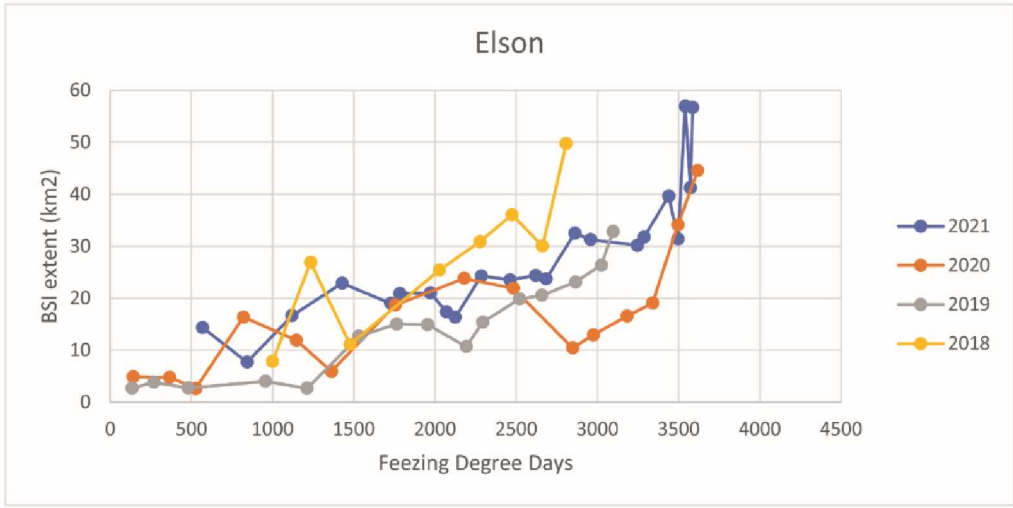
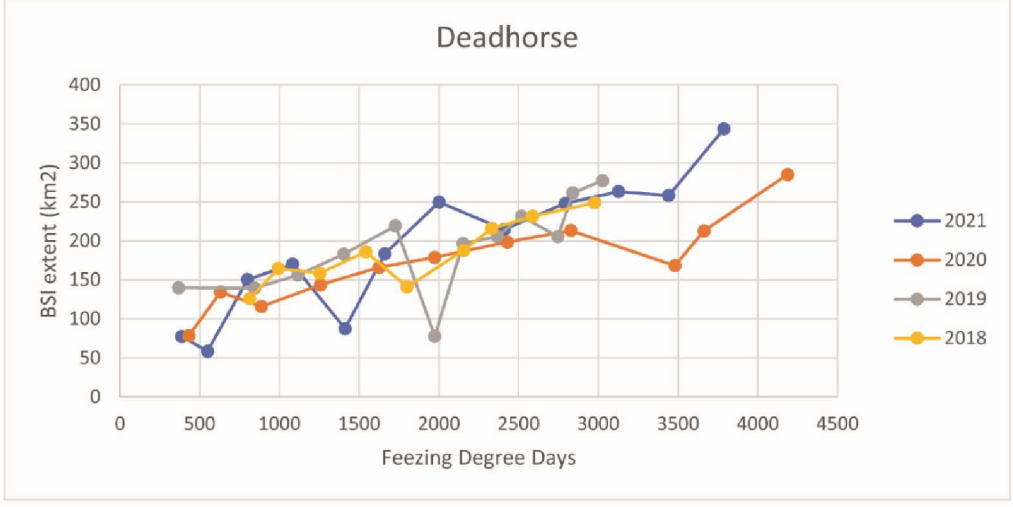
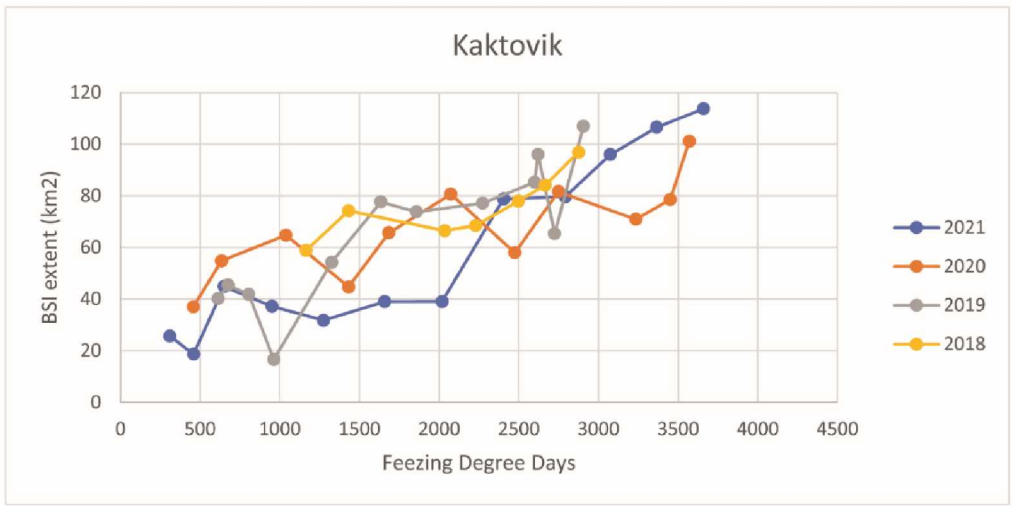
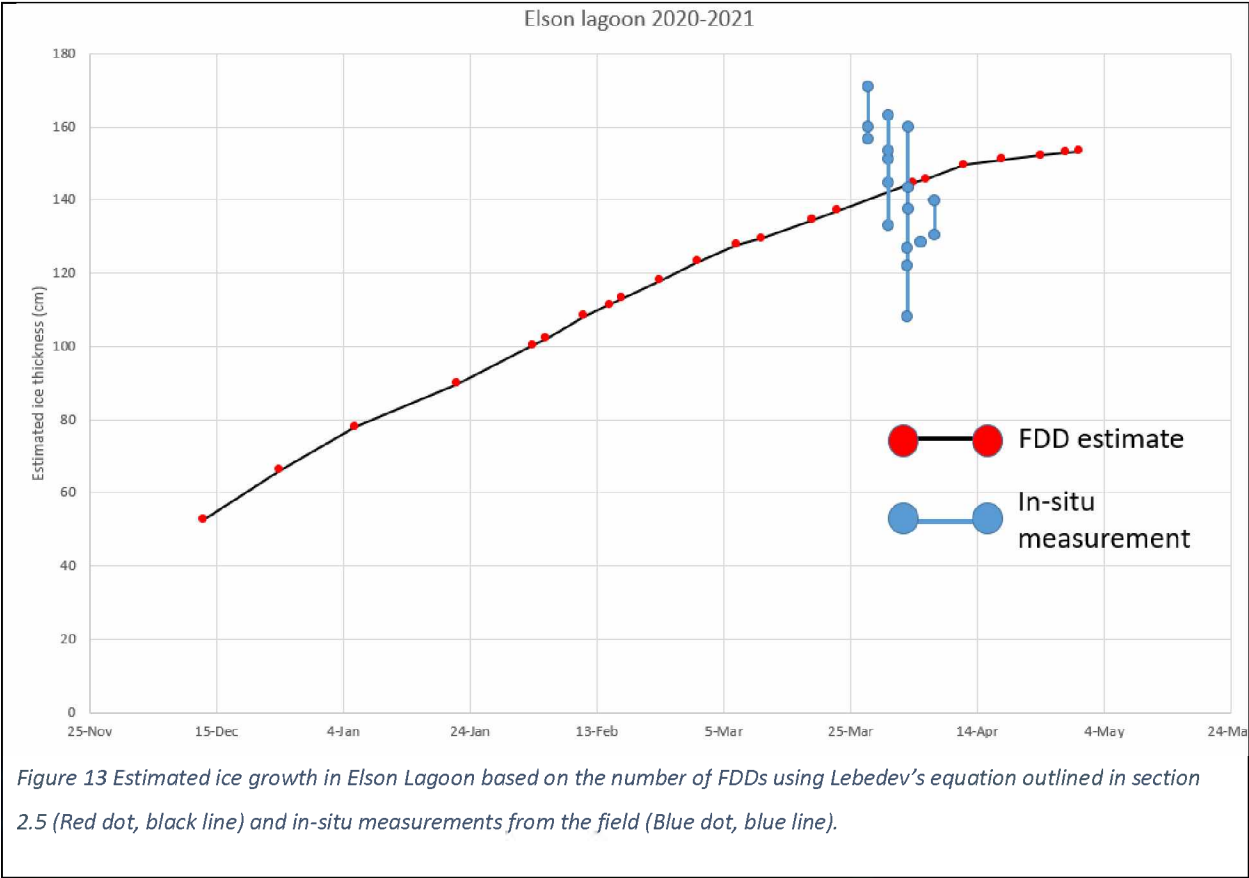
A**B****C**

Figure 12 Freezing degree day (FDD) calculations for each node. The x axis represents the total accumulation of FDDs and the y axis shows BSI extent in km² at the time. The amount of FDDs is variable year to year which shows up in the difference in length of each line.



3.2.2 Elson Lagoon

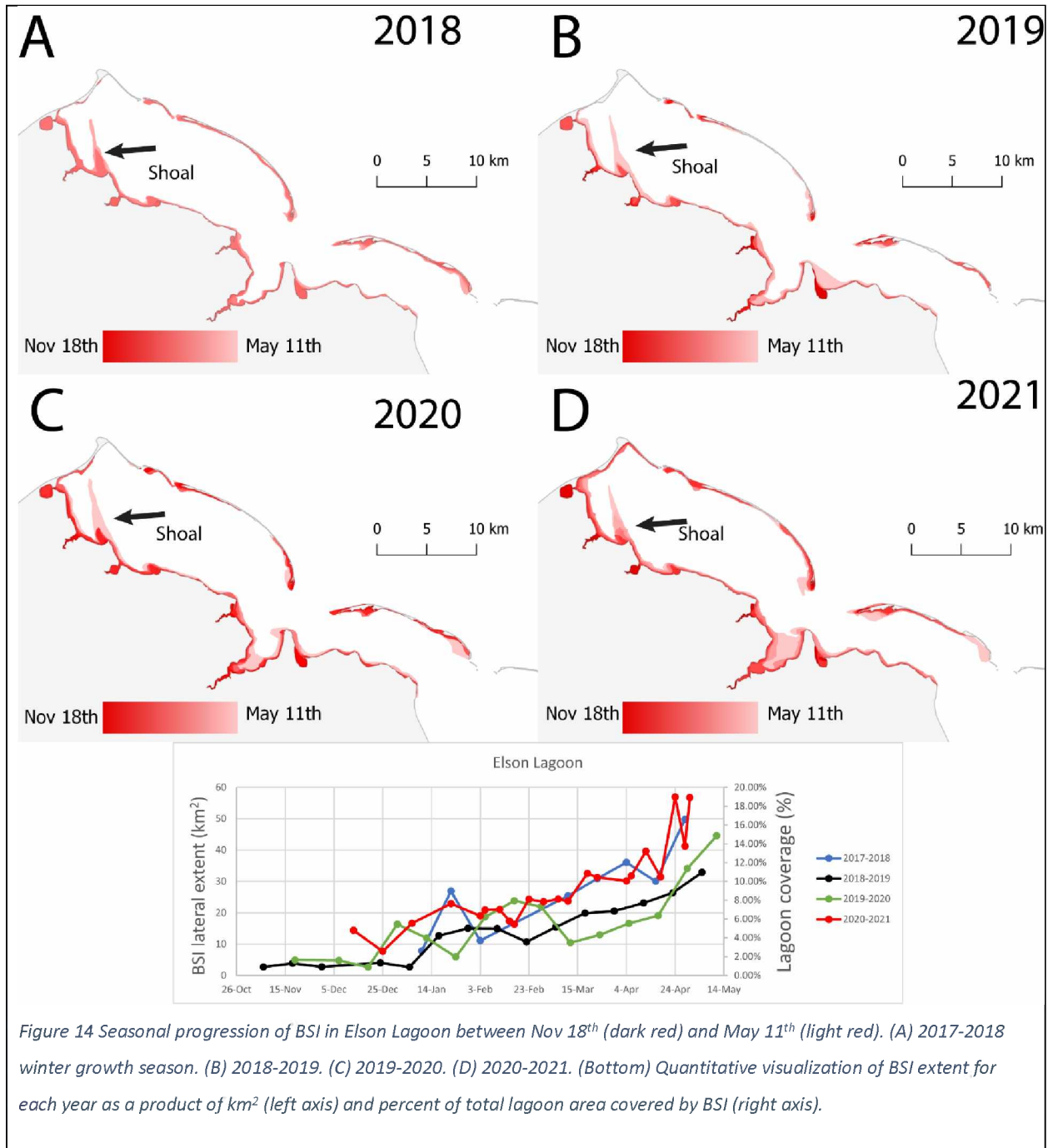


Figure 14 Seasonal progression of BSI in Elson Lagoon between Nov 18th (dark red) and May 11th (light red). (A) 2017-2018 winter growth season. (B) 2018-2019. (C) 2019-2020. (D) 2020-2021. (Bottom) Quantitative visualization of BSI extent for each year as a product of km² (left axis) and percent of total lagoon area covered by BSI (right axis).

During the seasonal progression of BSI from November to May through four winter cycles, the typical progression of BSI in Elson Lagoon starts first in drainage basins and in shallow regions along the coast before forming in the deeper parts of the lagoon (Figure 14). Late seasonal formation of BSI was also observed along the shoal in the western half of the lagoon extending north from Tekegakrok Point.

When BSI first appears and is at its minimum extent for each year, it occupies between 1 and 5% of the lagoon’s total area. Overall, BSI extent covers a relatively small fraction of Elson lagoon, with just under 20% of the total area at its most extent in 2021. Year 2019 was the least extensive year for BSI in Elson Lagoon, when at its maximum extent, BSI covered roughly 11% of the lagoon. BSI formed consistently in most areas of the lagoon every year; however, the southern shoreline of point Barrow was absent of BSI in all years except for 2021. As seen in figures 6-9 the sea ice/seafloor interface can be variable, and the underlying seafloor sediment was found to be frozen in some locations and unfrozen in others.

3.2.3 Simpson Lagoon and Stefansson Sound

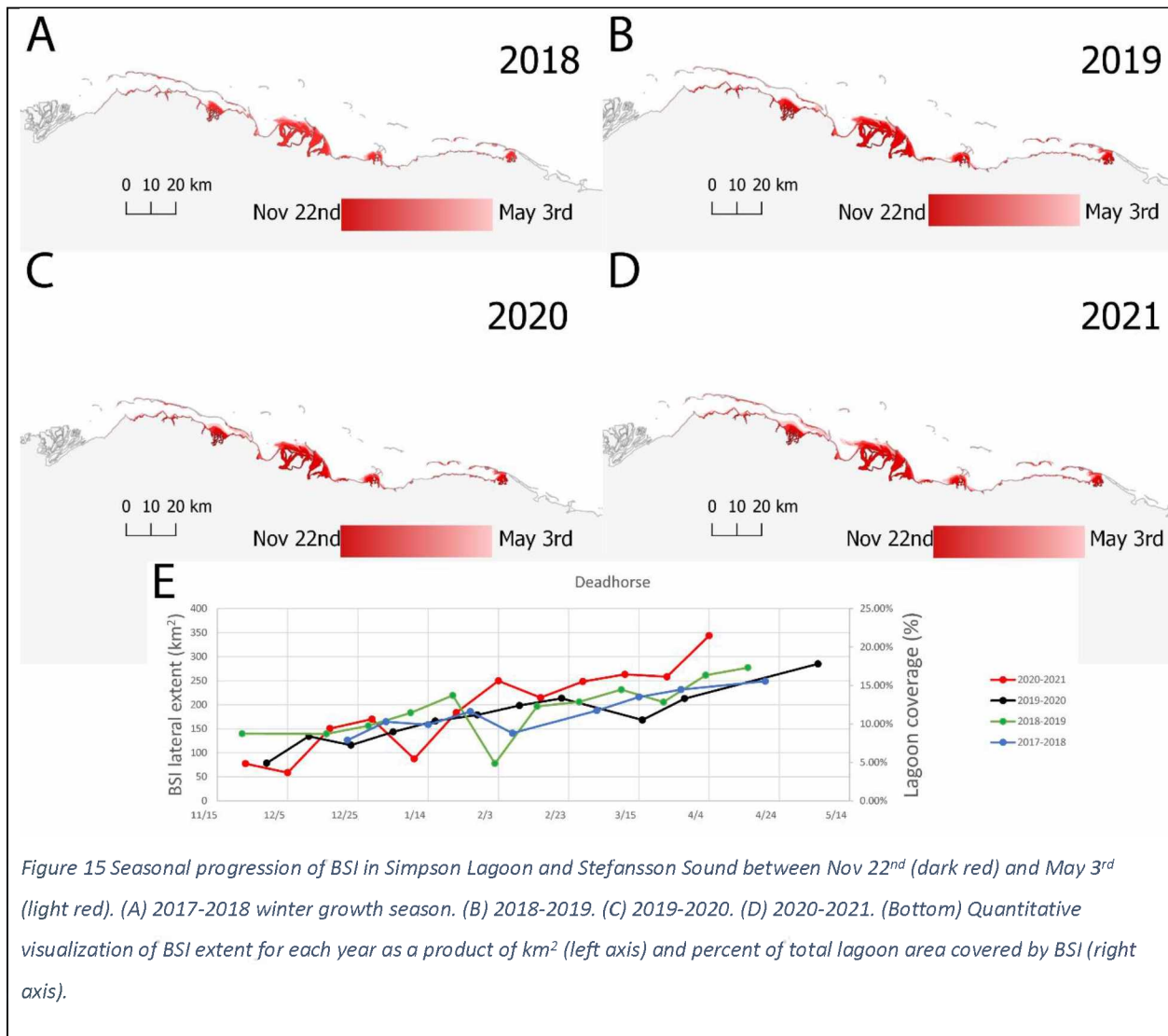
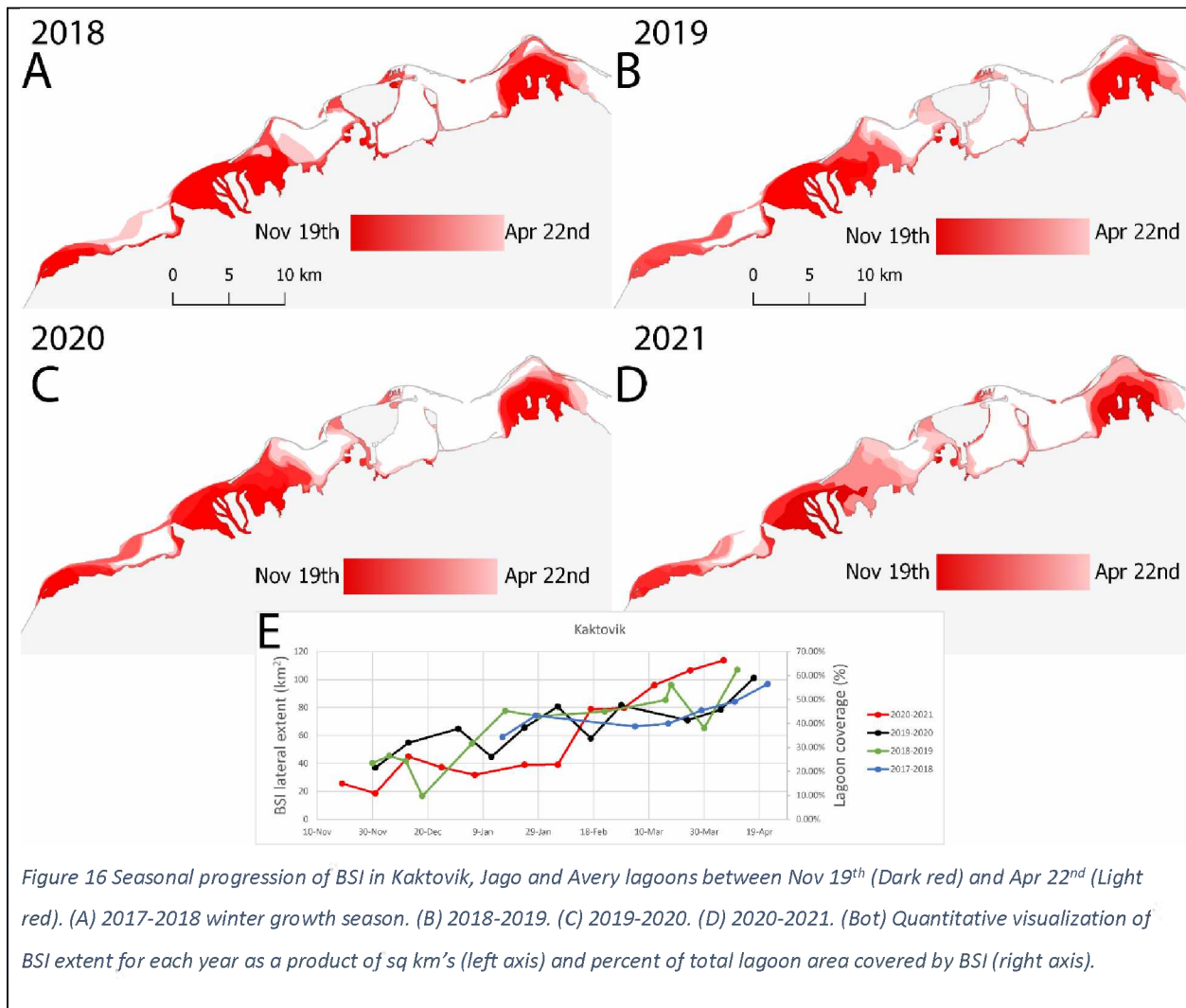


Figure 15 Seasonal progression of BSI in Simpson Lagoon and Stefansson Sound between Nov 22nd (dark red) and May 3rd (light red). (A) 2017-2018 winter growth season. (B) 2018-2019. (C) 2019-2020. (D) 2020-2021. (Bottom) Quantitative visualization of BSI extent for each year as a product of km² (left axis) and percent of total lagoon area covered by BSI (right axis).

BSI in the lagoons near the Deadhorse node first formed in river deltas in the early winter months and steadily increased in spatial extent, occupying deeper waters as the ice presumably thickened (Figure

15). BSI also formed along the coast in shallow regions, but this represented a small fraction of the total extent, which was dominated by BSI that formed near the river. Between the two lagoons there are four river deltas that account for the majority of BSI formation and there was a steady seaward progression of BSI throughout the winter. The extent of BSI during early in the winter season ranged from 5-10% of the total area of the lagoon. There was high variability in the timing and progression within each delta, depending on the ice growth that season; however, most years reached similar maximum extents between 15 and 23% of the total lagoons area.

3.2.4 Kaktovik, Jago, and Avery lagoons



Kaktovik, Jago and Avery lagoons make up the Kaktovik node and ice formation here also started in the river deltas (Figure 16), which collectively encompassed approximately 60% of the lagoon area. The

extent of BSI when it was first observed by InSAR each year ranged between 12 and 22% of the total lagoon area, except for the 2017-2018 season when SAR images were limited during the start of the winter growth period. BSI in this node occupied a much higher percentage of lagoon area respectively than at the other two nodes. However, the total area of BSI at its maximum, was roughly twice that at the Elson lagoon node, but still only half that at the Deadhorse node. As a result, by the end of the winter season, BSI that formed around the river deltas near at the Kaktovik node accounted for over half of the total area of the three lagoons while coastal BSI only accounted for roughly 10%. BSI in these river deltas expanded steadily throughout the winter and could extend as far as the barrier island at the opposite end of the lagoon by the end of the season. The seasonal progression of BSI was highly variable at this node and ice formation at the outer extents of the delta formed at different times each year while the maximum extent remained relatively consistent between 59 and 69% of the total lagoon area. BSI occupied the majority of Avery and Jago lagoons by the end of the growth season, while Kaktovik Lagoon remained mostly occupied by floating ice (Figure 16). This variability is likely related to the bathymetry of the lagoons, with Kaktovik Lagoon being deeper overall than the river delta-dominated waters of Jago and Avery lagoons.

3.3 Bottom fast ice core observations

The ice core collected at the location marked “ice sediment core #2” (Figure 5) in Elson Lagoon on April 27th, 2021, was retrieved with the contact between the bottom of the sea ice and the top of the frozen seafloor intact. The frozen interface demonstrates that there was a strong mechanical bond between the sea ice and the seafloor. With the upper ice surface at 0 cm, the first 43 cm were composed of sediment rich ice, indicating freezing of turbid water (Figure 17). In contrast, the ice between 43 cm and 51 cm was apparently sediment free, indicating ice growth in quiescent waters. The core broke during retrieval at the bottom of this layer of clean ice and the section of the core below contained the frozen interface between a 2-cm layer of sediment rich sea ice and the frozen seafloor at 53 cm below the upper ice surface. An 18-cm section of frozen seafloor sediment was recovered below the ice, resulting in a total core length of 71 cm. Three temperature measurements were taken: the first at the snow/ice interface, then near the mid-depth of the ice at 30 cm, and one at the bottom of the ice core at 51 cm (Figure 17).

An UBSI ice core was collected in Elson Lagoon, at the location marked “ice sediment core #1” in Figure 5 on April 25th, 2021. The upper 36 cm of this core contained a visibly large amount of sediment,

indicating turbid conditions during growth. Of this, the uppermost 22 cm were composed of granular ice, with columnar ice found throughout the core below (Figure 18). Immediately following the 36 cm mark, the rest of the ice core consisted of clean ice down to the bottom of the core at 90 cm, indicating ice growth in quiescent waters. The bottom of the ice core was in contact with frozen sediment; however, unlike the BBSI core it was not frozen to the seafloor and there was liquid water at the bottom of the hole once the core was retrieved. The water at the bottom of the hole had a temperature of -8.8°C . The temperature of the snow/ice interface at the top of the core was -8.2°C , at the bottom of the core it was -7.7°C , and down 10 cm into the frozen sediment the temperature was -7.8°C (Figure 18).

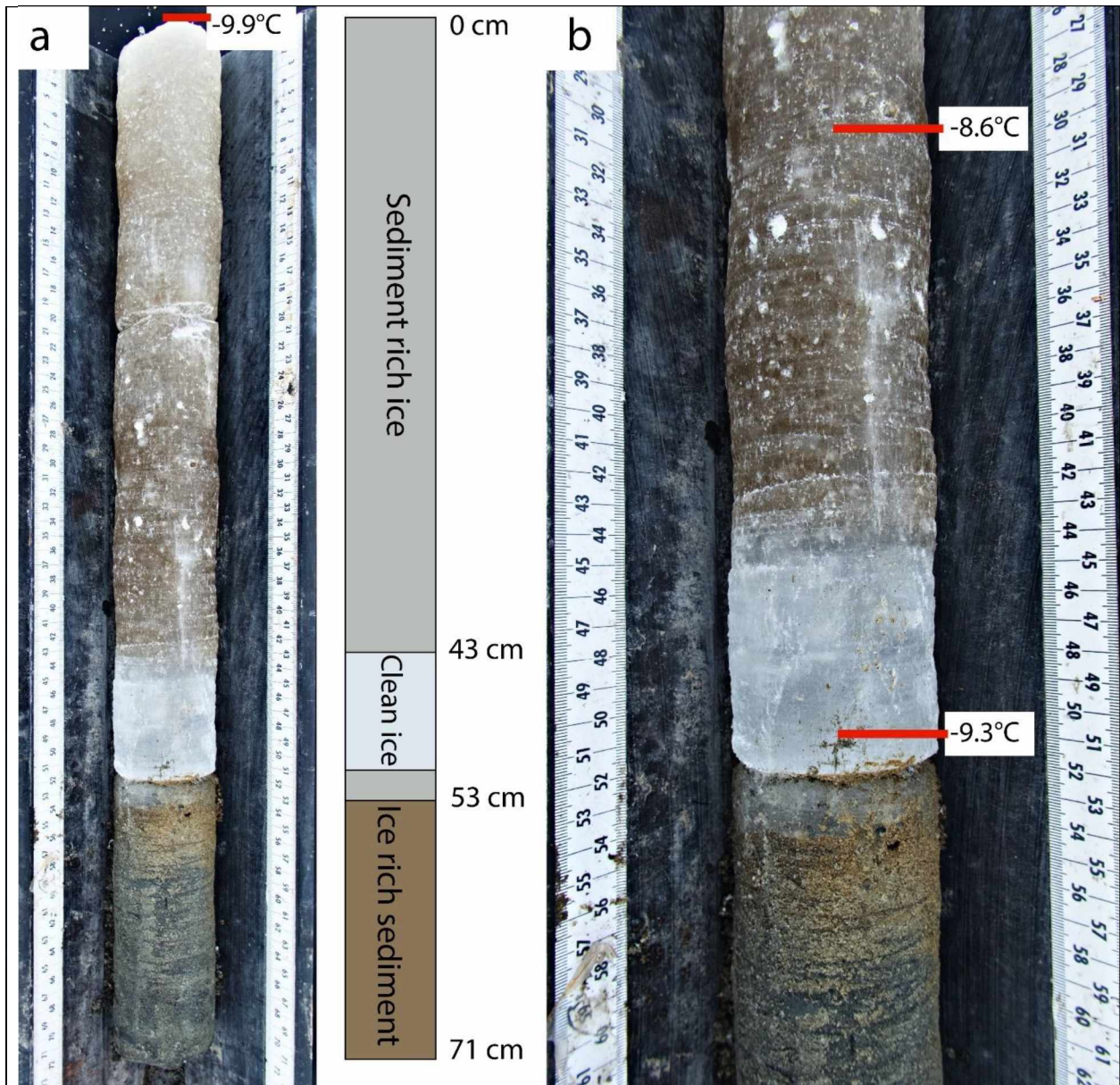


Figure 17 Sediment core collected near in Elson Lagoon at ice-sediment core #2 in Figure 5 April 27th, 2021. (a) Total core length is 71 cm, with 53 cm being BBSI and the remaining 18 cm being frozen sediment. (b) Closer view of the center of the ice core, which broke into two pieces upon retrieval above the ice/seafloor interface. Temperature reading line up next to where they were taken in the core. -9.9°C at the snow/ice interface, -8.6°C at 30 cm down core, -9.3°C at the bottom of the ice core, and air temperature at time of collection was -5.6°C.

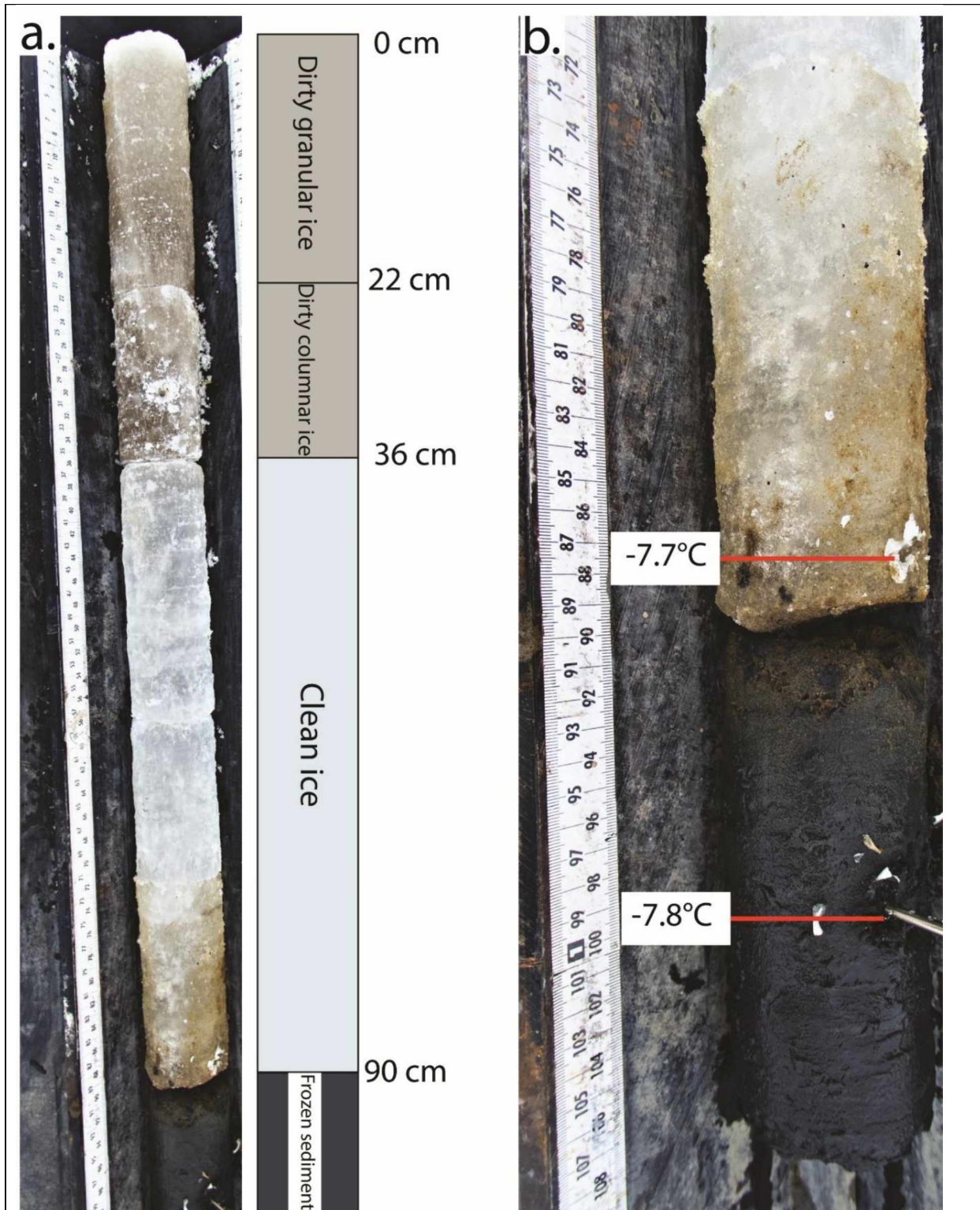


Figure 18 UBSI core collected in Elson Lagoon near ice sediment core #1 April 27th, 2021. (a) Total core length is 90 cm (b) Closer view of the bottom of the core. (b) Temperature reading line up next to where they were taken in the core. Temperature was -7.7°C at the bottom of the core, -7.8°C in the frozen sediment, and -8.2°C at the snow/ice interface.

4 Discussion

4.1 Validation of InSAR-derived BSI extent

4.1.1 Detection of BSI vs floating ice

We studied areas of BSI in coastal lagoons at three nodes along the Beaufort Sea coast (Figure 4) using interferometry. Three methods of BSI detection were used including in-situ ice auger measurements, EM conductivity surveys, and InSAR. Ground truthing data were collected at the Elson Lagoon study site only and are assumed to represent BSI validation across all other locations. Drill hole observations were made along four separate transects April 25th and May 5th, 2021, in Elson Lagoon, with two transects crossing the BSI zone from the coast to the floating ice and two transects crossing BSI over a shallow shoal that extends toward the center of the lagoon (Figure 5). These drill hole observations provided a definitive determination of whether the ice was BSI or floating. Additionally, they provided information about the nature of the seafloor/ice bottom interface, which is important when identifying whether the BSI is either bonded or unbonded and if the sediment beneath the ice is frozen. Along with drill hole observations, conductivity data were collected along the same four transects. The combination of these methods validated the ability of InSAR to detect the difference between BSI and floating ice

4.1.2 Distinction between bonded and unbonded BSI

The extensive in-situ drill-hole observations and ice cores collected across the BSI zone confirm the existence of both bonded and unbonded BSI in Elson Lagoon. The transitions in interferometric phase and coherence align most often with the boundary between UBSI and floating ice, as identified from drill holes (Figures 6-9). This demonstrates that, during the 12-day InSAR period corresponding to our field survey, any motion experienced by UBSI was significantly less than that which characterizes floating ice. However, it is possible that UBSI was mobile elsewhere in the study regions or at other times, such that the InSAR-derived BSI extent corresponds to that of BBSI. Episodic mobilization of UBSI may explain the intra-annual fluctuations in BSI extent observed in each season and in each lagoon system. With additional field observations throughout the year and in more locations, it may be possible to derive additional InSAR-based criteria for distinguishing between BBSI and UBSI, but we are not able to do so in this study.

BSI that forms in the shallowest regions close to shore experienced a far greater number of FDDs, allowing heat to be lost from the seafloor to support bonding (Table 1). The latest date a BBSI hole was detected was Mar 19th, 2021, in hole B4, and this hole was also the greatest depth at which BBSI was observed (1.29 m).

Drill holes	First observation of BSI	Number of FDDs while BSI	Amount of potential ice growth lost (m)	Ice thickness/water depth (m) Min-Max
C1, D1, D2, D3	Jan 22 nd 2021	2159	1.14	0.61-1.20
C2, D4	Feb 3 rd 2021	1858	1.04	0.80-1.17
C3, B6	Feb 15 th 2021	1516	0.93	0.63-0.91
B5, B7, B8, B9, B10, C4	Feb 23 rd 2021	1300	0.85	0.81-0.88
D5, D6, D7, D8	Mar 7 th 2021	966	0.71	1.10-1.30
B3, B4, B11, B12, B13, B14, B15, C5	Mar 19 th 2021	724	0.60	0.99-1.31
A7, A8, A9, A10, A11, A12, B16, B17	Apr 4 th 2021	340	0.39	0.87-1.24
A5, A6, A13, A14, A15	Apr 30 th 2021	0	0	1.21-1.37

Table 2 Date at which ice at each hole became bottomfast along with the number of subsequent FDDs after initial contact with the seafloor. The amount of potential ice growth lost due to grounding is shown in column 4, which uses the ice growth estimate equation outlined in section 2.5. The last column shows the range of water depth/ice thickness of the holes at which ice became bottomfast during that period.

The difference in FDDs can be seen when comparing transect A and B along the shallow shoal in Elson lagoon. The seasonal extent of BSI in this area shows that BSI formation occurs much earlier at the base of the shoal (Transect B) nearer to the coast than it does toward the crest (Transect A) further into the center of the lagoon in deeper waters. Figure 7a shows that the center of transect B has a continuous zone of BBSI, which likely explains why there is a consistent presence of BSI in that area after it is first detected by InSAR mapping. This is different from BSI along transect A, which formed late in the season in deeper waters and was found to be unbonded along the entire transect. UBSI along this transect transitions directly to and from floating sea ice along each side of the shoal, meaning that for InSAR to detect BSI at this location, the UBSI would have to have remained stable for at least 12 days, the cycle of

the satellite repeat orbit. This could mean that ice in this area had been in contact with the seafloor for a longer period than observed using InSAR methods as there could have been a change in the water level during the 12-day window, causing ice motion, making this region to appear as floating sea ice in the interferogram image.

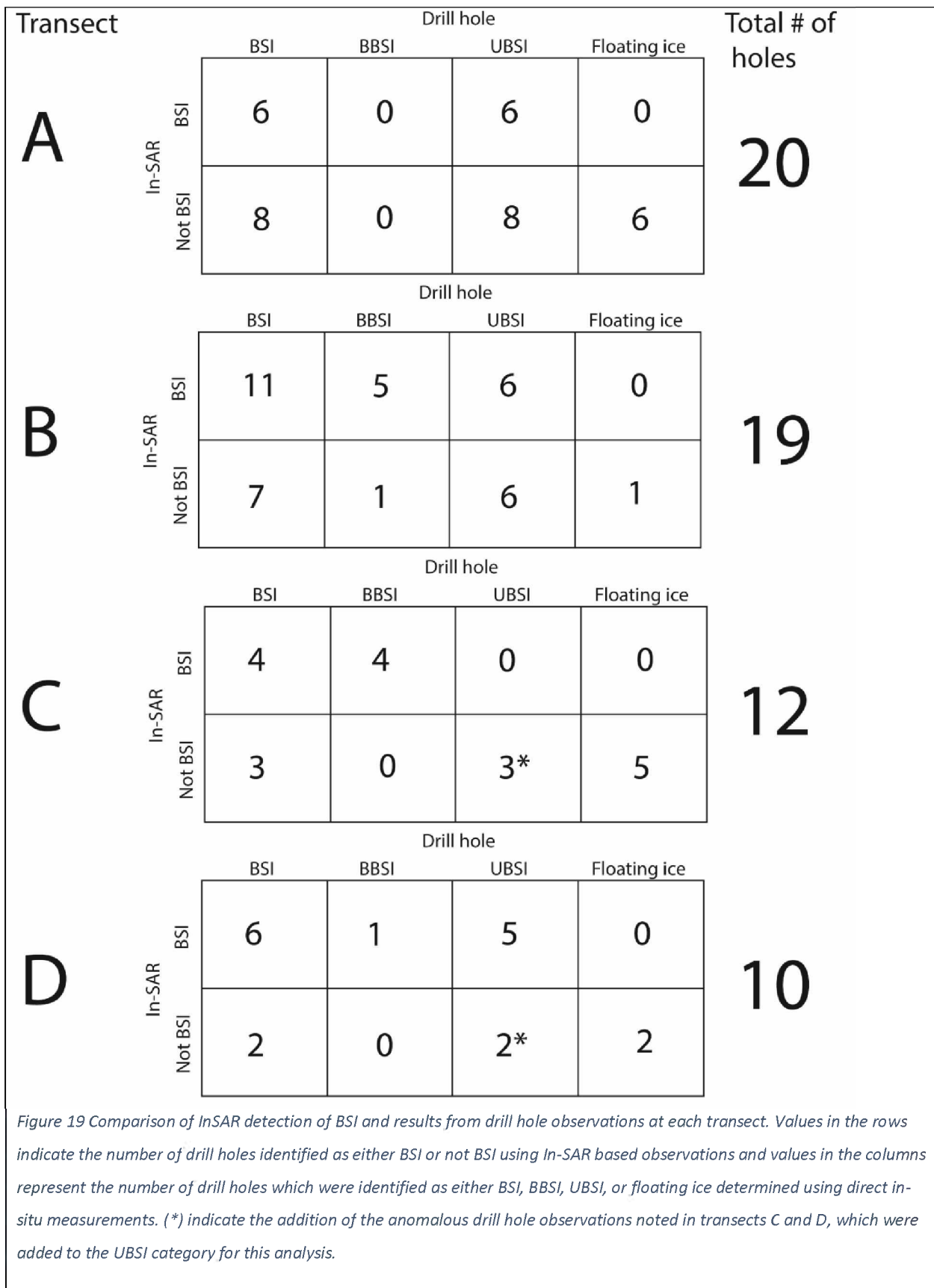


Figure 19 Comparison of InSAR detection of BSI and results from drill hole observations at each transect. Values in the rows indicate the number of drill holes identified as either BSI or not BSI using In-SAR based observations and values in the columns represent the number of drill holes which were identified as either BSI, BBSI, UBSI, or floating ice determined using direct in-situ measurements. (*) indicate the addition of the anomalous drill hole observations noted in transects C and D, which were added to the UBSI category for this analysis.

4.2 Assessment of EM conductivity profiling for detecting BSI

Our EMP-400 surveys did not reveal any distinguishable difference in apparent conductivity between BBSI and UBSI, despite the presence of highly saline brine at the ice/seafloor interface in regions of UBSI. Changes in conductivity occur most prominently when crossing from land-based measurements to those of nearshore BSI and then again when crossing from BSI to regions of floating sea ice. Short-scale variability in conductivity due to snow depth variations on top of the ice might be masking any small signals associated with the transition between BBSI and UBSI. Inner BSI conductivity variability could be caused by differences in seafloor sediment salinity between regions of frozen and unfrozen sediment bases. If sediment types affect conductivity readings, then it could be difficult to distinguish the conductivity difference between BBSI and UBSI. The combination of InSAR and conductivity profiling, however, does allow us to determine regions of UBSI quite well. As seen in figures 6-9, there are regions where phase values increase while conductivity values remain consistent with those of adjacent BSI as there is not a large enough presence of saltwater beneath the ice to trigger a spike in conductivity like one would see in the transition to a floating sea ice regime. With our in-situ auger measurements, we can see that the spike in conductivity is the most accurate method for identifying the difference between floating and BSI, while InSAR methods are best used to determine the difference between BBSI and floating sea ice.

4.3 Quality of detection for each observation method

4.3.1 Interferometric phase values

The detection of BSI purely using changes in phase seems to define a fairly accurate boundary along the nearshore; however, this method would appear to only capture a partial region along the shallow shoal extending from point Tekegakrok. This method is accurate in detecting the boundary of BBSI from UBSI though, which would make sense as UBSI is still subject to motion as it is not completely bonded to the seafloor.

4.3.2 Coherence values

The drop in coherence values align closely with the boundary between floating ice and BSI in the nearshore region and along the shallow shoal extending from point Tekegakrok. While this method alone does not match in-situ measurements exactly for each transect, it is much better at detecting

areas of UBSI than the observations based on phase alone. The ability to detect BSI with coherence values is most promising at the end of the growth cycle when BSI is at its maximum extent. However, coherence data from earlier in the season show inconsistencies in areas of suspected BSI. Additional analysis of coherence values across BSI in earlier winter months would be beneficial for future studies utilizing this method of observation.

4.3.3 Conductivity values

Conductivity measurements along each transect proved to be very accurate at detecting the transition from coastline to BSI and from BSI to floating sea ice. This method also proved efficient at detecting the amount of seawater beneath regions of floating ice. Conductivity values continued to increase as the profiler crossed into deeper waters and increases and decreases were consistent with known bathymetry values of Elson Lagoon. Conductivity values were not useful in detecting the difference between BBSI and UBSI though, and while we found there to be a thin layer of hypersaline seawater at the seafloor/ice interface, there was not a discernable difference in conductivity across the two types of BSI.

4.4 Spatial and temporal variation

By observing the area of BSI coverage and comparing it to total lagoon area we can calculate how much of the lagoon is represented by BSI throughout the season. This approach allows us to analyze seasonal variability as well as the interannual variability of BSI extent. Seasonal variability could be caused by differences in air temperature and timing and severity of snow fall and storm events, which can affect seasonal ice growth. BSI could be lifted from the seafloor if it was not in contact with the seafloor long enough to bond the two interfaces with enough strength to resist buoyancy forces caused by tidal variations. This could cause BSI to appear as floating ice using InSAR until later in the season after forming a stronger bond to the seafloor. UBSI is, therefore, underrepresented in this study as InSAR techniques are incapable of distinguishing between these two types of ice (Figure 19). As UBSI is likely underrepresented in our data, the total area of BSI shown in Figures 14 – 16 should be taken as conservative estimate of the amount of ice in contact with the seafloor at any time.

The amount of BSI that forms each year also depends on the size and morphology of the lagoon system. Even though the area of Elson Lagoon is much larger than the combined area of the lagoons within the Kaktovik node, Elson Lagoon forms 50 km² of BSI, which is approximately half the area that forms in the

three Kaktovik lagoons (100 km²). Elson Lagoon contains no major river deltas, but it does have a significant shallow shoal feature in the western half of the lagoon, which accounts for a large portion of BSI formation. The formation of BSI on this shoal occurs much later in the season than in river deltas of other lagoons, which means BSI formation is first seen along the coast at Elson Lagoon. Deadhorse lagoons are large (1725 km²) and contain four major river deltas, which account for the majority of the 300 km² of BSI formation that forms each year. River deltas are going to be the primary location for the formation of BSI and lagoons with river deltas are going to see an early winter freeze up and steady BSI growth throughout the winter.

The proximity of the barrier islands to the river delta plays a major factor in BSI formation as there is a chance to bridge two separate BSI formations, which could lead to an overestimate of BSI that might offset under-detection of UBSI. As BSI forms on the lagoon side of the barrier islands and is adjacent to the seaward progression of BSI sourced from river deltas the two stable regions could lock the floating ice into place which could be falsely identified as BSI using our InSAR method alone. While the barrier islands are not close enough to any BSI formation in Elson lagoon (9 km), both Deadhorse and Kaktovik lagoons have nearby barrier islands that are connected by BSI (3 km). If BSI formed on the barrier islands merges with the BSI that forms from the river delta, there could be an ice bridge that gets locked into place inhibiting motion and causing floating ice to be identified as BSI by InSAR interpretation.

Deltas that are not confined by proximal barrier islands tend to have rapid growth of BSI to a maximum extent initially and then a slower rate of expansion later in the season. This could be caused by the bathymetry of delta being very shallow near the shore and tapering out to a more inclined slope at the distal end. The increase in water depth would mean that ice would only be able to form at the further extents if ice thickness were higher that year. Other factors could be the timing of tidal forces on UBSI as it could be lifted from the seafloor just prior to bonding and be identified as floating ice for that 12-day interferogram before appearing bottomfast in the next.

When we compared percent coverage of BSI for each lagoon, Elson and Deadhorse lagoons trend closely and are typically within 10% of each other and with a maximum extent of between 10-20% of the total lagoon area. Kaktovik lagoons have a significantly higher percent of lagoon coverage, reaching as high as 50-60% of the entire lagoon at its maximum detectable extent. BSI formation in Kaktovik lagoons leaves less than half of the total area of the lagoon free of ice gouging effects and could have additional effects on saltwater accumulation at peak ice formation. By seeing where BSI forms early in the season one could track changes using InSAR to identify shallow barrier islands or observe coastline changes.

4.5 Submarine permafrost impacts

On average, the maximum annual extent of BSI across all three lagoon systems amounts to ~450 km². This is, therefore, the area of the seafloor that becomes thermally connected to the atmosphere, allowing the submarine permafrost to cool below the freezing point of the ocean. Shallow areas with BSI formation early in the winter have prolonged contact and thermal exchange between the atmosphere and submarine permafrost layers. Submarine permafrost coming into thermal contact with BSI in November-December could be coupled to atmospheric conditions for as long as 5 months during peak winter conditions. BSI that forms later in the season will have a lesser impact on submarine permafrost preservation as the duration of coupling will be reduced as the end of the season approaches. Figure 13 shows FDDs compared with amount of BSI formed at each location. It does not matter how many FDDs had occurred prior to BSI contacting that region, it matters how many occur after it forms. Once BSI forms then it can cool the upper layer of submarine permafrost, which can reduce the thickness of the active layer that grows when in contact with warmer ocean water the rest of the year. Detectable BSI appears first in the shallowest areas of the lagoon systems, and most commonly at river deltas, where there are large areas of shallow water. These areas are going to be where the most submarine permafrost is preserved while areas in deeper waters that do not have BSI formation until the end of the year will preserve the least amount of near-seabed submarine permafrost.

4.6 Ecological impacts

BSI can have profound impacts on seafloor communities as it creates inhospitable living conditions seasonally. BSI freezes the entire water column, leaving no open water for organisms to overwinter. In regions just outside of BSI, conditions in the thin layer of water left between the ice and the seafloor are hyper saline, which is lethal for most organisms. The extent of BSI is different for each lagoon as Elson and Deadhorse nodes only see ~20% of the seafloor with BSI at the end of the winter while in Kaktovik lagoons, BSI can cover as much as 70% of the total seafloor area. This would mean that all the organisms inhabiting the seafloor during the rest of the year would need to occupy the remaining 30% until spring. Some organisms were found to be overwintering in the frozen sediment beneath the ice in Elson lagoon, which would mean that they buried themselves before the sediment froze and waited out the ice prior to returning to the seafloor surface.

Conclusion

This study has found that there is a distinct difference between the two types of BSI and that we are able to identify and map these two regions accurately as either BBSI or UBSI. By identifying these two ice types as unique we can better understand how each impact and affect their surroundings. For example, identifying regions of BBSI would be beneficial for industrial ice road construction as BBSI is significantly more stable as it is completely frozen to the seafloor as opposed to UBSI, which is still subject to motion. The regions of BBSI will better preserve submarine permafrost in its immediate area as heat is removed from the seafloor as soon as the ice is bonded. Areas outside of the BBSI zone would have greater rates of active layer thickening and degradation of the submarine permafrost, which would make the upper layers of sediment less stable. As this shoreward migration of BSI extent occurs, shallow submarine permafrost levels will also move shoreward as more regions of the seafloor experience year-round exposure to seawater and the active layer continues to increase in thickness within larger areas around the coast. The decrease in submarine permafrost could allow for a large amount of methane to be released into the atmosphere, and these nearshore regions where we find BBSI will be highly susceptible to large increases in permafrost degradation in the near future.

From an ecological perspective, the difference between ice that rests on the seafloor and ice that is in frozen contact with the seafloor could be the difference between a habitable region and one that is inhospitable for most organisms to overwinter in. We found that some regions of UBSI have frozen sediment beneath it but that is not true for the majority of UBSI. If the sediment is not frozen then burrowing organisms could potentially overwinter in the upper sediment layers instead of relocating to deeper waters. Organisms found inactive in frozen sediment samples regained activity once the sediment thawed, which means that if they were able to dig into the sediment before it froze then they could overwinter here.

As sea ice continues to thin in the Arctic, BSI will be one of the first impacted and the nearshore regions will likely see significant changes as the stability provided by BSI diminishes. We will likely see the BBSI zone continue to migrate towards the coast as regions that were once BBSI become UBSI and regions that were UBSI would become floating sea ice. The nearshore region should be monitored closely for changes in accordance with the degradation of BSI and, more importantly, the transition from regions that were once BBSI to UBSI or floating sea ice. Continued InSAR observations within the three node systems would be highly valuable and easy to accomplish in order to identify variations from year to

year. Additionally, this method could be used across the entire Beaufort Sea coastline and does not have to be restricted to the three node systems chosen for this study. For a long-term effort of established monitoring is desired an automated process of identifying the difference between BSI and floating sea ice would be the ideal route to take. EM surveying across the same tracks taken at different times during the winter season could provide a greater understanding of the early-stage progression of BSI as well as the yearly changes of extent. EM surveys would greatly benefit from similar collections across the other node locations and across the river deltas. This method can cover a large area in a short time and can be employed extensively across in the nearshore region. Following these two methods concentrated drill hole observations in areas of interest could be beneficial to further verify the accuracy of the two non-invasive methods.

References

- Angelopoulos, M., P. P. Overduin, F. Miesner, M. N. Grigoriev, and A. A. Vasiliev (2020), Recent advances in the study of Arctic submarine permafrost, *Permafrost and Periglacial Processes*, 31(3), 442-453.
- Dammann, L. E. Eriksson, A. R. Mahoney, C. W. Stevens, J. Van der Sanden, H. Eicken, F. J. Meyer, and C. E. Tweedie (2018), Mapping Arctic bottomfast sea ice using SAR interferometry, *Remote Sensing*, 10(5), 720.
- Dammann, D. O., H. Eicken, F. J. Meyer, and A. R. Mahoney (2016), Assessing small-scale deformation and stability of landfast sea ice on seasonal timescales through L-band SAR interferometry and inverse modeling, *Remote Sensing of Environment*, 187, 492-504, doi: <http://dx.doi.org/10.1016/j.rse.2016.10.032>.
- Docquier, D., and T. Koenigk (2021), Observation-based selection of climate models projects Arctic ice-free summers around 2035, *Communications Earth & Environment*, 2(1), 1-8.
- Eicken, H., I. Dmitrenko, K. Tyshko, A. Darovskikh, W. Dierking, U. Blahak, J. Groves, and H. Kassens (2005), Zonation of the Laptev Sea landfast ice cover and its importance in a frozen estuary, *Global and planetary change*, 48(1-3), 55-83.
- Haas, C., S. Gerland, H. Eicken, and H. Miller (1997), Comparison of sea-ice thickness measurements under summer and winter conditions in the Arctic using a small electromagnetic induction device, *Geophysics*, 62(3), 749-757.
- Hallikainen, M., and D. P. Winebrenner (1992), The physical basis for sea ice remote sensing, *Microwave remote sensing of sea ice*, 68, 29-46.
- Hogenson, K., S. A. Arko, B. Buechler, R. Hogenson, J. Herrmann, and A. Geiger (2016), Hybrid Pluggable Processing Pipeline (HyP3): A cloud-based infrastructure for generic processing of SAR data, paper presented at AGU Fall Meeting Abstracts.
- Mahoney, A., H. Eicken, A. G. Gaylord, and L. Shapiro (2007), Alaska landfast sea ice: Links with bathymetry and atmospheric circulation, *Journal of Geophysical Research: Oceans*, 112(C2).
- Moreira, A., P. Prats-Iraola, M. Younis, G. Krieger, I. Hajnsek, and K. P. Papathanassiou (2013), A tutorial on synthetic aperture radar, *IEEE Geoscience and Remote Sensing Magazine*, 1(1), 6-43, doi: 10.1109/MGRS.2013.2248301.
- Osterkamp, T. (2001), Sub-sea permafrost, *Elements of Physical Oceanography: A Derivative of the Encyclopedia of Ocean Sciences*, 2, 2902-2912.

Overduin, P. P., S. Liebner, C. Knoblauch, F. Günther, S. Wetterich, L. Schirrmeister, H. W. Hubberten, and M. N. Grigoriev (2015), Methane oxidation following submarine permafrost degradation: Measurements from a central Laptev Sea shelf borehole, *Journal of Geophysical Research: Biogeosciences*, 120(5), 965-978.

Overduin, P. P., S. Wetterich, F. Günther, M. N. Grigoriev, G. Grosse, L. Schirrmeister, H.-W. Hubberten, and A. Makarov (2016), Coastal dynamics and submarine permafrost in shallow water of the central Laptev Sea, East Siberia, *The Cryosphere*, 10(4), 1449-1462.

Perovich, D., W. Meier, M. Tschudi, S. Hendricks, A. Petty, D. Divine, S. Farrell, S. Gerland, C. Haas, and L. Kaleschke (2020), Arctic report card 2020: Sea ice.

Solomon, S. M., A. E. Taylor, and C. W. Stevens (2008), Nearshore ground temperatures, seasonal ice bonding, and permafrost formation within the bottom-fast ice zone, Mackenzie Delta, NWT, paper presented at Proceedings of the Ninth International Conference on Permafrost, Fairbanks, Alaska.

Stevens (2011), Controls on Seasonal Ground Freezing and Permafrost in the Near-Shore Zone of the Mackenzie Delta, NWT, Canada.

Stevens, B. J. Moorman, and S. M. Solomon (2010), Interannual changes in seasonal ground freezing and near-surface heat flow beneath bottom-fast ice in the near-shore zone, Mackenzie Delta, NWT, Canada, *Permafrost and Periglacial Processes*, 21(3), 256-270.

Stroeve, J. C., M. C. Serreze, M. M. Holland, J. E. Kay, J. Malanik, and A. P. Barrett (2012), The Arctic's rapidly shrinking sea ice cover: a research synthesis, *Climatic change*, 110(3), 1005-1027.

Tibbles, M., J. A. Falke, A. R. Mahoney, M. D. Robards, and A. C. Seitz (2018), An InSAR habitat suitability model to identify overwinter conditions for coregonine whitefishes in Arctic lagoons.